Chapter 5

# Role of tungsten coordination and valence states in $ZnF_2$–$WO_3$–$TeO_2$ glasses on the emission features of $Nd^{3+}$, $Sm^{3+}$ and $Eu^{3+}$ ions in the visible and IR spectral ranges

*The glasses of the composition (45-x) $ZnF_2$–x $WO_3$–49$TeO_2$:1.0 $Nd_2O_3$/$Sm_2O_3$/$Eu_2O_3$ with x varying from 5 to 20 mol% were synthesized. Optical absorption, fluorescence spectra (in the spectral range 400–2300 nm) and also fluorescence decay were studied at ambient temperature. The Judd-Ofelt theory analysis was applied to characterize the absorption and luminescence spectra of $Ln^{3+}$ ions in these glasses. Following the luminescence spectra, various radiative properties like transition probability A, branching ratio $\beta$ and the radiative life time $\tau$ for $^4F_{3/2} \rightarrow {}^4I_{11/2}$, $^4G_{5/2} \rightarrow {}^6H_{7/2}$, $^5D_0 \rightarrow {}^7F_2$ emission levels respectively for $Nd^{3+}$, $Sm^{3+}$ and $Eu^{3+}$ doped glasses of these glasses have been evaluated. The variations observed in these parameters were discussed following of varying co-ordinations (tetrahedral and octahedral positions) and the valence states of tungsten ions in the glass network. A significant enhancement in the intensities of $^4F_{3/2} \rightarrow {}^4I_{11/2}$ ($Nd^{3+}$), $^4G_{5/2} \rightarrow {}^6H_{7/2}$ ($Sm^{3+}$) and $^5D_0 \rightarrow {}^7F_2$ ($Eu^{3+}$) emission lines has been observed with increase of $WO_3$ content; this is attributed to the increase in the concentration $W^{5+}$ ions in the glass net work that acts as modifiers. The quantitative analysis of these results (with the aid of the data on ESR, IR and Raman spectral studies) has indicated that the glasses mixed with around 15 mol% of $WO_3$ have the optimum concentration for yielding the highest quantum efficiency with low phonon losses for the above mentioned principal transitions.*

# Role of tungsten coordination and valence states in $ZnF_2$–$WO_3$–$TeO_2$ glasses on the emission features of $Nd^{3+}$, $Sm^{3+}$ and $Eu^{3+}$ ions in the visible and IR spectral ranges

## 5.1 Introduction

Tellurium oxide based glasses are well known due to their high density, high transparency in the mid infrared region (~5.0–11.0 μm), high linear and nonlinear refractive index, good stability against moisture as mentioned in earlier chapters. In view of such qualities these glasses are highly suitable for hosting rare earth ions since they provide a low phonon energy (~ 750 nm, lower than geramanate, phosphate and silicate glasses) environment that minimizes non-radiative losses [1–8]. The presence of tungsten ions in these glasses, further, makes them suitable for optoelectronic devices since they exhibit photochromism and electrochromism properties. Tungsten ions are expected to have profound influence on luminescence characteristics of rare earth ions in tellurite glasses, for the simple reason that these ions exist in different valence states viz., $W^{6+}$, $W^{5+}$ and also in $W^{4+}$ as per the following thermo reversible disproportionate reaction:

$$W^{5+} + W^{6+} \leftrightarrow W^{4+} + W^{6+}$$

regardless of the oxidation state of the tungsten ion in the starting glass batch [9–13].

Among these, $W^{6+}$ ions participate in the glass network with different structural units like $WO_4$ ($T_d$) and $WO_6$ ($O_h$). The $WO_4$ units form the linkages

of the type Te–O–W with $TeO_4$ and $TeO_3$ structural units in the glass network since the electronegativities (2.1 for Te ion and 2.0 for $W^{6+}$ ion) are very close to each other. On the other hand $W^{5+}$ ($5d^1$) ions forming the complexes of $W^{5+}O_3^-$, act as modifiers and induce structural disorder in the tellurite network by transforming $TeO_4$ to $TeO_{3+1}$ structural units in the glass network. Hence, the varying concentration of $WO_3$ in the glass network results varying environment of luminescent ions present in the tellurite glass network. As a consequence, interesting changes in the luminescent characteristics of lasing ions is expected.

The study on absorption and emission characteristics of $Nd^{3+}$ ($4f^3$) ion has been subject of extensive investigation in a number of crystalline and glass materials because of its prospective applications in NIR laser technology [14–18]. The transition $^4I_{9/2} \rightarrow {}^2P_{1/2}$ (around 430 nm) in the absorption spectra is a characteristic of coordination of this ion. Generally this band is desirable in the construction of compact and efficient laser source pumped by diode laser. The impact of changing environment in the glass network due to the variation in the concentration of the tungsten ions is expected to very high on this transition.

Samarium containing glasses are known to have an unusual elastic behaviour due to valance instability [19]. This ion exists in trivalent and divalent states but between these two states, $Sm^{3+}$ ($4f^5$) is found to be more stable. Samarium exhibits promising characteristics for spectral hole burning

studies [20, 21]. The decay of exited states in $Sm^{3+}$ involves different mechanisms depending on the matrix. Earlier studies on optical absorption, fluorescence and life-time measurements of $Sm^{3+}$ ions in oxyfluoroborate and oxide glasses have indicated the quenching of the fluorescence of $^4G_{5/2}$ level [22, 23]; this is attributed to quadrupole-quadrupole interaction among the samarium ions. Similarly, a number of earlier studies on spectroscopic properties of $Sm^{3+}$ ions in different glass matrices have revealed that the fluorescence yield of this rare earth ion is strongly dependent on its environment inside the glass network [24-29].

Europium ion, another interesting rare earth ion, has got variable valency states, $Eu^{3+}$ and $Eu^{2+}$. $Eu^{3+}$ ($4f^6$ ion) is quite stable even at high temperatures in crystalline and glassy host matrices. The transitions, $^7F_0 \rightarrow {}^5D_2$ in the absorption spectrum and $^5D_0 \rightarrow {}^7F_2$ in the emission spectrum of $Eu^{3+}$ are reported to be hypersensitive; the integrated emission intensity ratio of $^5D_0 \rightarrow {}^7F_2$ (red) and $^5D_0 \rightarrow {}^7F_1$ (orange) transitions (R/O ratio) is strongly influenced by site asymmetry and covalency of the bonds with the ligand anion [30, 31]. The effect of surrounding ions on the luminescence of europium in glass has been reported in several works [32–34] which clearly indicated that the relative intensities of the $Eu^{3+}$ emission peaks depend strongly on the variations in the glass network at the vicinity of this ion. $Eu^{3+}$ ion has the additional feature of interest; phonon side band studies can give information

about the electron-phonon coupling strength with the host lattice and also throw light whether, non-radiative or radiative decay is favoured.

The thorough literature survey on $TeO_2$ glasses as laser host materials, indicates that though some considerable number of studies on $WO_3$-$TeO_2$ glasses are available [35, 36], still there is a lot of scope to investigate the influence of the tungsten ions on the emission characteristics of rare earth ions. In view of this it is felt worth while to investigate the fluorescence features of three different rare earth ions viz., $Nd^{3+}$, $Eu^{3+}$ and $Sm^{3+}$ ions in the visible and infrared regions in $ZnF_2$–$WO_3$–$TeO_2$ glass system with the gradual increase of $WO_3$ content in the glass network at the expense of $ZnF_2$. The results of ESR, IR and Raman spectral studies have also been used to have a comprehensive pre-knowledge over the structural changes in the glass network due to the variations in the concentrations of $WO_3$ at the vicinity of rare earth ions which influence the luminescence efficiency.

## 5.2 A brief review on the spectroscopic studies of $Nd^{3+}$, $Sm^{3+}$ and $Eu^{3+}$ ions in various glass systems

### $Nd^{3+}$ glasses:

Surendra Babu *et al.* [37] have recently reported the results of their studies on 1.06 μm emission in $Nd^{3+}$-doped alkali niobium zinc tellurite glasses. From this study they have concluded that $^4F_{3/2} \rightarrow {}^4I_{11/2}$ is the probable lasing transition excited with low threshold power. Cankaya and Sennaroglu [38] have reported lasing emission of $Nd^{3+}$ ions in $TeO_2$–$WO_3$ glasses at 1.37

μm. In this report the authors have claimed to have measured the luminescence efficiency as much as 78%. Saleem *et al.* [39] have reported optical absorption and near infrared emission properties of $Nd^{3+}$ ions in alkali lead tellurofluoroborate glasses. In this study the authors have evaluated total radiative transition probabilities ($A_T$), stimulated emission cross-sections ($\sigma_E$) and gain bandwidth parameters ($\sigma_E \times \Delta\lambda P$) and compared with the earlier reports. Zhong *et al.* [40] have reported 2.7 μm emission of $Nd^{3+}$, $Er^{3+}$ codoped tellurite glass. In this study the authors have observed the enhanced mid infrared emission due to the co-doping. Verma *et al.* [41] have studied effect of modifiers ($BaF_2$ $BaCl_2$ and $BaCO_3$) and heat treatment on the fluorescence bands of $Nd^{3+}$ ions in $TeO_2$ glasses. Their study has indicated that the $BaCl_2$ modified glass exhibits maximum upconversion intensity among the three modifiers. From the temperature dependent fluorescence studies of these glasses the authors have concluded that $Nd^{3+}$ doped tellurite glass can be used as a temperature sensor.

Courrol *et al.* [42] have studied spectral properties of lead fluoroborate glasses doped with $Nd^{3+}$. Wilhelm *et al.* [43] have reported the fluorescence life time enhancement of $Nd^{3+}$-doped sol–gel glasses by Al–codoping and $CO_2$-laser processing. Karthikeyan and Mohan [44] have reported the structural, optical and glass transition studies on $Nd^{3+}$ doped lead bismuth borate glasses. Annapurna *et al.* [45] have investigated the NIR emission and

upconversion luminescence spectra of $Nd^{3+}$:$ZnO–SiO_2–B_2O_3$ glasses. Saisudha and Ramakrishna [46] have found large radiative transition propabilities in bismuth borate glasses doped with $Nd^{3+}$ ions. Shen *et al.* [47] have reported the compositional effects and spectroscopy of rare earths ($Er^{3+}$, $Tm^{3+}$, and $Nd^{3+}$) in tellurite glasses. Kumar *et al.* [48] have explored the stimulated emission and radiative properties of $Nd^{3+}$ ions in barium fluorophosphate glass containing sulphate. Chen *et al.* [49] have studied ion-implanted waveguides in $Nd^{3+}$ doped silicate glass and $Er^{3+}/Yb^{3+}$ co-doped phosphate glass. Kam and Buddhudu [50] have studied Luminescence enhancement in ($Nd^{3+}$+$Ce^{3+}$) doped $SiO_2$: $Al_2O_3$ sol-gel glasses. Rosa-Cruz *et al.* [51] have reported the results of their study on spectroscopic characterization of $Nd^{3+}$ ions on barium fluoroborophosphate glasses. Fernandez *et al.* [52, 53] have evaluated the upconversion losses in Nd-doped fluoroarsenate glasses. Surana *et al.* [54] have investigated the Laser action in neodymium-doped zinc chloride borophosphate glasses. Vijaya Prakash reported [55] his results of absorption spectral studies of Pr, Nd, Sm, Dy, Ho and Er ions doped in NASICON type phosphate glass, $Na_4AlZnP_3O_{12}$. Rao *et al.* [56] have reported luminescence properties of $Nd^{3+}$: $TeO_2–B_2O_3–P_2O_5–Li_2O$ glass. Xiang *et al.* [57] have studied the up-conversion emission in violet from yellow in $Nd^{3+}$: $SiO_2–TiO_2–Al_2O_3$ sol-gel glasses. Bouderbala *et al.* [58] have reported the results of their studies on infrared and visible room temperature fluorescence induced by

continuous laser excitation of new $Nd^{3+}$: phosphate glasses. Cassanjes *et al.* [59] have investigated Raman scattering, differential scanning calorimetry and $Nd^{3+}$ spectroscopy in alkali niobium tellurite glasses. Mehta *et al.* [60, 61] have investigated the spectroscopic properties including ESR of $Nd^{3+}$ doped phosphate and borate glasses. Kumar and Bhatnagar [62] have reported the effect of modifier ions on the covalency of $Nd^{3+}$ ions in cadmium borate glasses. Srinivasa Rao *et al.* [63] have reported the physical and absorption properties of $Nd^{3+}$ doped mixed alkali fluoro-borophosphate optical glasses. Ajit Kumar *et al.* [64] have reported the spectroscopic parameters of $Nd^{3+}$ ion in phosphate glasses. Joshi and Lohani [65] have investigated the non-radiative energy transfer from $Tm^{3+}$ to $Ho^{3+}$ and $Nd^{3+}$ in zinc phosphate glass. Dawar *et al.* [66] have studied the optical and acousto-optical properties of Nd: phosphate glasses. Ning Lei *et al.* [67] have fabricated Ti: sapphire laser pumped Nd: tellurite glass laser. Pozza *et al.* [68] have investigated the absorption and luminescence spectroscopy of $Nd^{3+}$ and $Er^{3+}$ in a zinc borate glass. Ratnakaran and Buddhudu [69] have reported the optical absorption spectra and laser analysis of $Nd^{3+}$ ions in fluoroborate glasses. Sen and Stebbins [70] have studied structural role of $Nd^{3+}$ in $SiO_2$ glass using NMR studies. Ebendorff *et al.* [71] have studied the spectroscopic properties of $Nd^{3+}$ ions in phosphate glasses.

## $Sm^{3+}$ glasses:

Shanmuga Sundari *et al.* [72] have reported composition dependent structural and optical properties of $Sm^{3+}$ doped sodium borate and sodium fluoroborate glasses. In this study the authors have observed that the radiative parameters are decreasing with the decrease in the sodium content in the glass. Agarwal *et al.* [73] have reported radiative properties of $Sm^{3+}$ ions doped zinc bismuth borate glasses. In this study the variations of intensity parameters, radiative transition probabilities observed with variation in the content of $Bi_2O_3$ in the glass network have been discussed in detail. Sooraj Hussain *et al.* [74] have reported absorption and emission characteristics of $Sm^{3+}$ and $Dy^{3+}$ in lithium boro tellurite glasses. In this study the authors have reported a bright orange ($^4G_{5/2} \rightarrow {}^6H_{7/2}$) along with a red ($^4G_{5/2} \rightarrow {}^6H_{9/2}$) and a yellow ($^4G_{5/2} \rightarrow {}^6H_{5/2}$) emission transitions of $Sm^{3+}$ ions. Udaya Bhaskar *et al.* [75] prepared the $sm^{3+}$ doped $BiO_2$-$B_2O_3$-$Li_2O$ glass and examined the absorption, excitation and lifetimes of different measured emission bands. Biju *et al.* [76] have investigated up conversion fluorescence in $Sm^{3+}$-doped zinc phosphate glassy matrix. Jayasankar *et al.* [77] have studied optical properties of $Sm^{3+}$ ions in zinc and alkali zinc borosulphate glasses and they also [78] studied fluorescence spectra and decay properties of the $^4G_{5/2}$ level of the $Sm^{3+}$ions in lithium borate and lithium fluoroborate glasses as a function of the pressure up to 27.2 and 25.9 G Pa respectively, at room temperature. Kumar *et al.* [79]

have observed stark splitting in the upper and lower levels in the fluorescence and measured the life-time of $^4G_{5/2}$ level as a function of $sm^{3+}$ ion concentration. Kojima *et al.* [80] have prepared and studied optical spectroscopy 0f 79.5 $ZnCl_2$-10 $BaCl_2$-10 KCl-glasses containing divalent and trivalent samarium ions. Souza Filho *et al.* [81] have investigated the high pressure dependence of $Sm^{3+}$ emission in PbO-$PbF_2$-$B_2O_3$ glasses. Annapurna *et al.* [82] reported the optical characterization of $Sm^{3+}$ doped silicate glass from the measurements of optical absorption spectra at (300K), total luminescence spectra fluorescence life times in the temperature range (10–300K) of the prominent emission transitions. Mahapatra [83] studied optical absorption and photoluminescence for $Sm^{3+}$ ions doped (in the range 8.7 x $10^{19}$ to 7.8x $10^{20}$ ions $cm^{-3}$) calcium metaphosphate glasses. He analysed the spectral intensities in terms of the Judd-Ofelt parameters $\Omega_{\lambda}$. Shimizugava *et al.* [84] have studied LIII XANES before and after X–ray or UV irradiation. XANES in this edge showed that a part of trivalent ion converted to divalent ion upon the irradiation of X-ray. Shimizugava *et al.* [85] have studied X–ray absorption fine structure of samarium –doped glasses using synchrotron radiation. Farries *et al.* [86] reported the laser emission at 651 nm in a $Sm^{3+}$ -doped silica optical fibre in a Fabri-Perot type laser cavity.

## $Eu^{3+}$ glasses:

Kassab *et al.* [87] have recently reported influence of metallic nanoparticles on electric-dipole and magnetic-dipole transitions of $Eu^{3+}$ doped germanate glasses. Their results have suggested that the magnetic response of rare–earth doped metal-dielectric composites at optical frequencies can be as strong as their electric response due to the confinement of the optical magnetic field. Zhu *et al.* [88] have reported the influence of thermal treatment on optical and structure properties of europium-doped $SiO_2$–$HfO_2$ glasses. In this study the authors have measured fluorescence line narrowing spectra for the samples sintered at different temperatures were measured, and the results were interpreted in terms of structural changes in the glass matrix and the $Eu^{3+}$ bonding environment. Liu [89] has studied the effect of $Eu^{3+}$ ions concentration on the optical properties $TeO_2$-BaO-$Eu_2O_3$ glass. In this study the author has observed that the absorption intensity increases relative to that of the host with the increase of the $Eu^{3+}$ ions concentration. Xu *et al.* [90] have reported optical properties of $Bi^{3+}$: $Eu^{3+}$ codoped borosilicate glass. In this study the authors have observed that $Bi^{3+}$ ions act as sensitizers and enhances the luminescence intensity of $Eu^{3+}$ in this glass system. Carmo *et al.* [91] have reported thermo-optical properties of tellurite glasses doped with $Eu^{3+}$ and gold nanoparticles. In this study luminescence of $Eu^{3+}$ ions in the yellow-red region was examined as a function of Au nanoparticles concentration. The influence

of the nanoparticles concentration on the thermal diffusivity of the glass and the $Eu^{3+}$ luminescence is also discussed in detail. Kam at al. [92] have reported the spectroscopic properties of some heavy metal oxide glasses doped with $Eu^{3+}$. Wasylak *et al.* [93] have reported IR optical limiting in europium and thulium doped oxide glasses. Biju *et al.* [94] have studied the energy transfer in $Sm^{3+}$-$Eu^{3+}$ co-doped system in zinc sodium phosphate glasses. Fragosoa *et al.* [95] have investigated the luminescence and energy transfer processes in borate glasses using luminescence spectroscopy. Awomir *et al.* [96] have measured the absorption and emission spectra of $Eu^{3+}$ and $Dy^{3+}$ ions in $Li_2B_4O_7$ glasses grown in oxygen and hydrogen gas. Lavin *et al.* [97] have analysed in detailed the optical properties of $Eu^{3+}$ ions in calcium diborate glasses to correlate them with the local environment of the lanthanide ions in these glasses. Kushida *et al.* [98] have analysed the spectral shape of the $^5D_0 \rightarrow {}^7F_0$ line of $Eu^{3+}$ and $Sm^{2+}$ in glass. Reddy *et al.* [99] have studied the spectroscopic properties of $Eu^{3+}$ ions in the $B_2O_3$–$AlF_3$–RF (where R=Li, Na, K) glasses. Akshaya Kumar *et al.* [100] have recorded and analysed absorption and fluorescence spectra of $Eu^{3+}$ ions doped in a tellurite glass. Xia et al [101] have prepared and studied optical spectroscopy of $Li_2O$–$Al_2O_3$–$SiO_2$ glasses containing divalent and trivalent europium ions. Annapurna *et al.* [102] have presented the results concerning the excitation and emission spectra of 1 mol % $Eu^{3+}$-doped $50ZnCl_2$–$20BaCl_2$–29KCl glass. Silversmith *et al.* [103] have

measured the fluorescence line narrowing and emission decay measurements on $Eu^{3+}$ doped sol gel glasses. Sooraj Hussain *et al.* [104] have prepared and studied the emission spectra of europium-doped germanium–lead bismuth based glasses. Kityk [105] and his co workers have recently reported red luminescence studies in $Eu^{3+}$ doped heavy metal oxide glasses. They have found that only excitation by the polarized photoexcitation Ar pulsed laser light ($\lambda$= 528 nm) gives a substantial increase of red luminescence with $\tau$ = 1320 μs. Babu *et al.* [106] have investigated optical spectroscopic properties of $Eu^{3+}$ ions in lithium borate and lithium fluoroborate glasses. Culea *et al.* [107] have reported the structural and magnetic behaviour of some borate glasses containing $Eu^{3+}$ ions. Bettinelli *et al.* [108] reported the spectroscopic investigations of zinc borate glasses doped with $Eu^{3+}$ ions. Aruna *et al.* [109] have studied the spectral properties of $Eu^{3+}$: $B_2O_3$–$P_2O_5$–$R_2SO_4$ glasses, (where R = Li, Na and K). Vaz *et al.* [110] have synthesized and investigated the spectroscopy and crystallization behavior of $Eu^{3+}$–doped $La_2O_3$:$B_2O_3$ binary glasses. Jagannathan *et al.* [111] have synthesized nano–crystallites in $Eu^{3+}$–doped zinc boro–sulphate glasses and studied the luminescence properties of these glasses.

## 5.3 Results

The composition (50-x)$ZnF_2$–x$WO_3$–49$TeO_2$: 1$Ln_2O_3$ (with x ranging from 5 to 20) is chosen for the present study. The details of the composition are:

$LnW_5$: 45$ZnF_2$–5$WO_3$–49$TeO_2$:1$Ln_2O_3$

$LnW_{10}$: 40$ZnF_2$–10$WO_3$–49$TeO_2$:1$Ln_2O_3$

$LnW_{15}$: 35$ZnF_2$–15$WO_3$–49$TeO_2$:1$Ln_2O_3$

$LnW_{20}$: 30$ZnF_2$–20$WO_3$–49$TeO_2$:1$Ln_2O_3$

where Ln = Nd, Sm and Eu.

From the measured values of density d and calculated average molecular weight $\overline{M}$, various physical parameters such as rare earth ion concentration $N_i$ and mean Ln ion separation $r_i$ of these glasses are evaluated using the conventional formulae and are presented in Table 5.1.

SEM pictures and X-ray diffraction pattern of the $ZnF_2$–$WO_3$–$TeO_2$: $Ln_2O_3$ glass samples showed no signs of crystallinity, indicating the prepared samples were of amorphous in nature. The chemical makeup of the glasses is evaluated using EDS. In Fig. 5.1, EDS of one of the glass samples in each series viz., $LnW_{10}$: 40$ZnF_2$–10$WO_3$–49$TeO_2$:1 $Ln_2O_3$ are presented; the analysis indicates the presence of Te, Zn, O, F, W, Nd, Sm and Eu elements in the glass samples.

**Table 5.1** Physical parameters of $ZnF_2$–$WO_3$–$TeO_2$: $Ln_2O_3$ glasses.

| Physical Parameter | $Nd^{3+}$ doped glasses | | | | $Sm^{3+}$ doped glasses | | | | $Eu^{3+}$ doped glasses | | | |
|---|---|---|---|---|---|---|---|---|---|---|---|---|
| | $NdW_5$ | $NdW_{10}$ | $NdW_{15}$ | $NdW_{20}$ | $SmW_5$ | $SmW_{10}$ | $SmW_{15}$ | $SmW_{20}$ | $EuW_5$ | $EuW_{10}$ | $EuW_{15}$ | $EuW_{20}$ |
| Density d ($g/cm^3$) | 5.505 | 5.616 | 5.726 | 5.837 | 5.525 | 5.636 | 5.746 | 5.857 | 5.618 | 5.729 | 5.839 | 5.950 |
| Molar volume $V_m$ ($cm^3$/mole) | 25.37 | 26.02 | 26.63 | 27.23 | 25.30 | 25.95 | 26.57 | 27.16 | 24.89 | 25.53 | 26.14 | 26.74 |
| Refractive index ($n_d$) | 1.501 | 1.502 | 1.502 | 1.503 | 1.504 | 1.505 | 1.506 | 1.507 | 1.512 | 1.514 | 1.515 | 1.515 |
| $Ln^{3+}$ ion conc. $N_i$ ($10^{19}$ ions/$cm^3$) | 1.19 | 2.31 | 3.39 | 4.42 | 1.19 | 2.32 | 3.40 | 4.43 | 1.21 | 2.36 | 3.46 | 4.50 |
| Inter-ionic distance $r_i$ (nm) | 9.44 | 7.56 | 6.66 | 6.09 | 9.44 | 7.55 | 6.65 | 6.09 | 9.38 | 7.51 | 6.61 | 6.06 |
| Polaron radius $r_p$ (nm) | 3.81 | 3.05 | 2.68 | 2.45 | 3.78 | 3.03 | 2.67 | 2.44 | 3.80 | 3.04 | 2.68 | 2.45 |

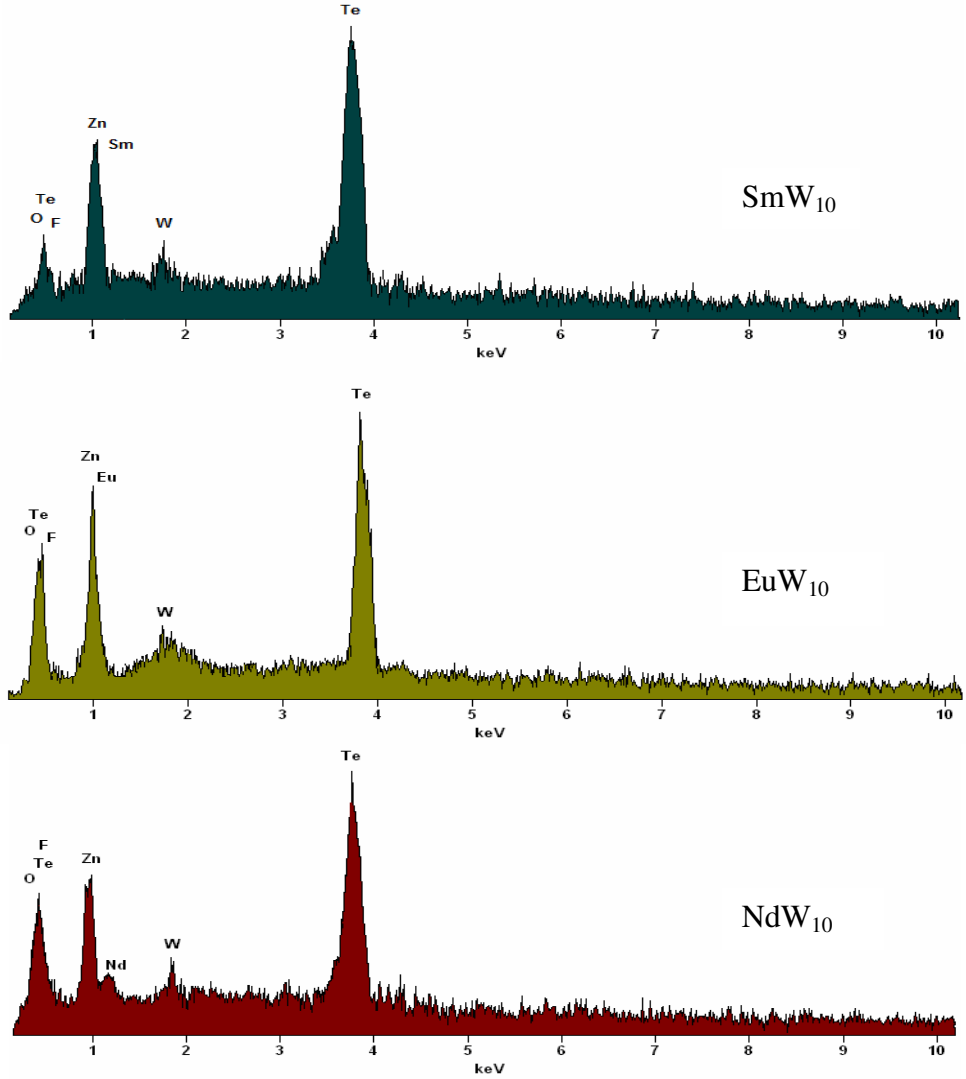


**Fig. 5.1** Energy dispersive spectra of $ZnF_2$–$WO_3$–$TeO_2$: $Ln_2O_3$ glasses mixed with 10 mol% of $WO_3$.

In Fig. 5.2, differential scanning calorimetric (DSC) scans of $ZnF_2$–$WO_3$–$TeO_2$ glass doped with $Nd_2O_3$ are presented. The trace of the glass $NdW_5$ exhibited an endothermic effect due to glass transition at about 300 $^oC$ followed by a well–defined exothermic effect due to crystallization temperature ($T_C$). The trace also exhibited another endothermic effect due to melting at 620 $^oC$. The variation of glass transition temperature ($T_g$), and glass forming ability parameter $K_{gl} = (T_C–T_g)/(T_m–T_C)$ with concentration of $WO_3$ for the three rare earth doped glasses are shown as inset of Fig. 5.2. The variation shows a downward kink at 15 mol% of $WO_3$.

Fig. 5.3 shows infrared transmission spectra of $ZnF_2$–$WO_3$–$TeO_2$: $Sm_2O_3$ glasses. The spectra exhibited different absorption bands due to various structural units of $TeO_2$ and $WO_3$. IR spectrum of crystalline $TeO_2$ (inset of Fig. 5.3) exhibited two absorption bands at 772 $cm^{-1}$ [$\nu_1(A_1)$] and at 650 $cm^{-1}$ [$\nu_2(A_2)$] due to $\nu_s$-$TeO_{2eq}$ and $\nu_s$-$TeO_{2ax}$ vibrations with $C_{2v}$ symmetry, respectively [112]. In the spectrum of glass $SmW_5$ (Fig. 5.3), the vibrational frequency of $\nu_s$-$TeO_{2ax}$ (axial band) is located at 645 $cm^{-1}$ whereas the $\nu_s$-$TeO_{2eq}$ is observed to be missing. Additionally, the spectrum of this glass exhibited the bands due to $\nu_1$ and $\nu_4$ vibrations of $WO_4$ groups at 936 and 421 $cm^{-1}$ respectively and also a feeble band at about 966 $cm^{-1}$ due to $\nu_1$ vibrations of $WO_6$ groups [113]. As the concentration of $WO_3$ is increased, the band due to $WO_6$ group is observed to grow at the expense of band due to $WO_4$ groups.

The symmetrical equatorial band of $TeO_2$ is also observed to decay gradually with the increase in the concentration of the $WO_3$ at least up to 15 mol%. A similar behaviour is exhibited by the spectra of other two series of glasses.

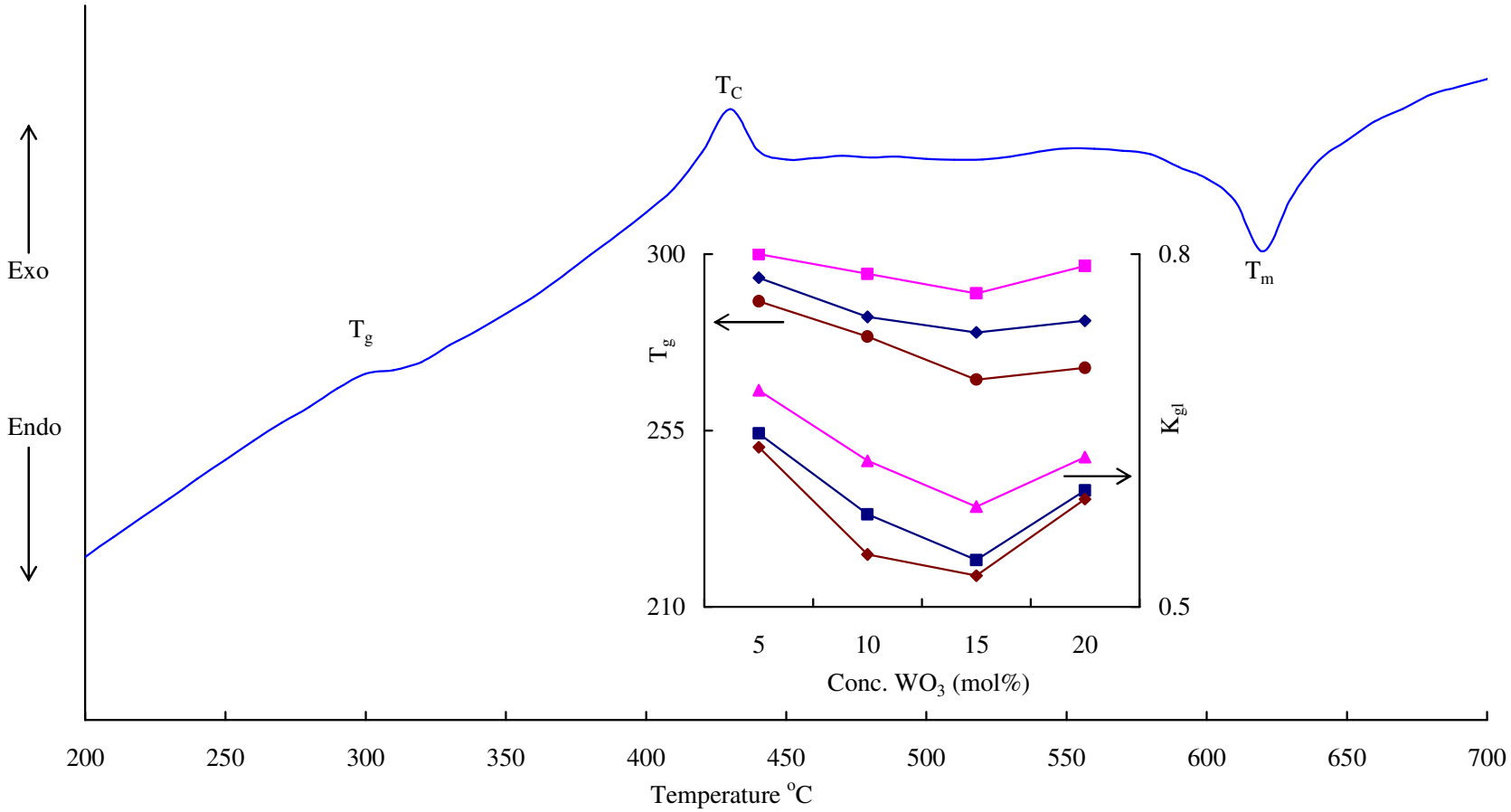


**Fig. 5.2** Differential scanning calorimetric (DSC) scan of $ZnF_2$–$TeO_2$:$Nd_2O_3$ glass mixed with 10 mol % of $WO_3$. Inset represents variation of glass forming ability parameter with the concentration of $WO_3$ for the three rare earth doped glasses.

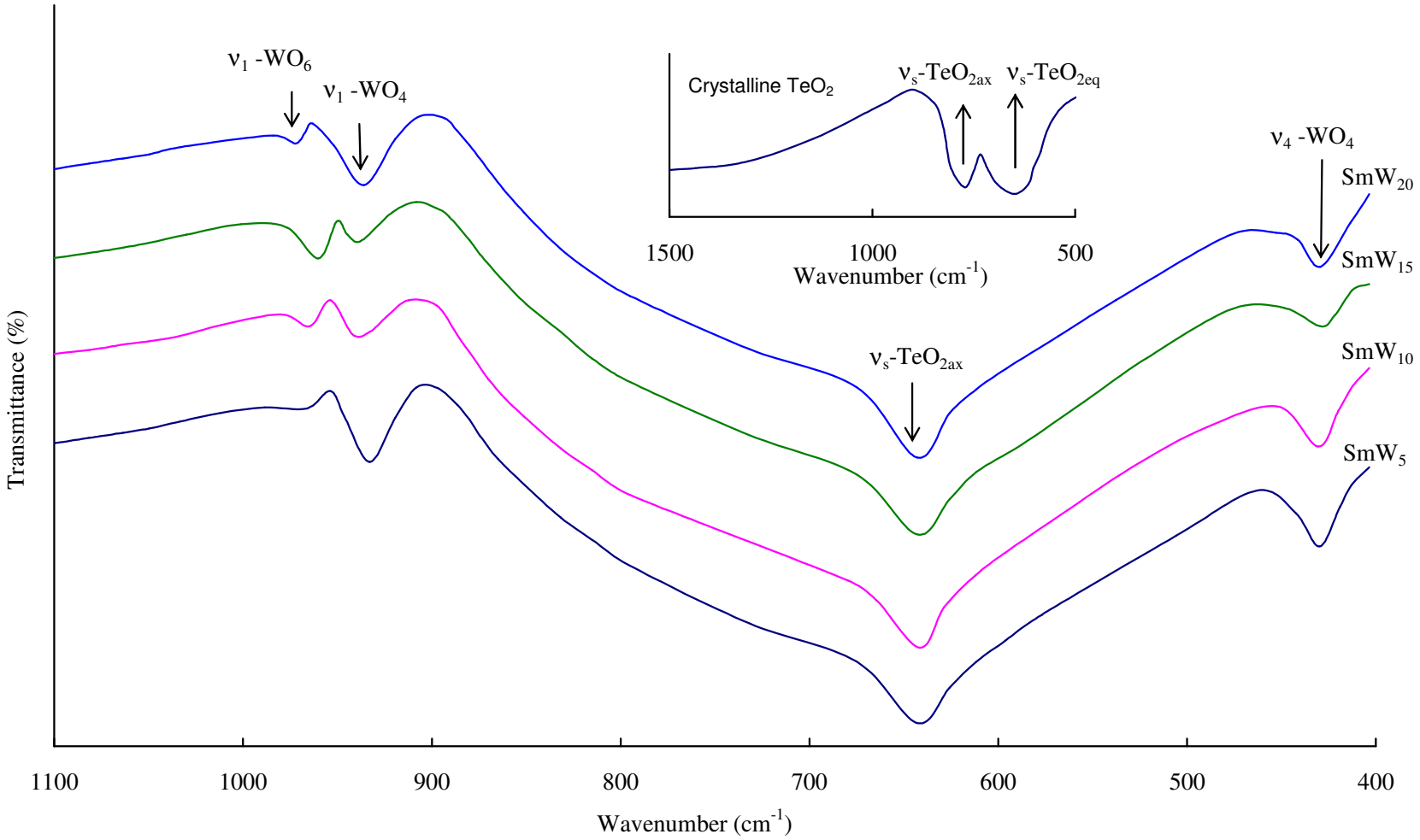


**Fig. 5.3** IR spectra of $ZnF_2$–$WO_3$–$TeO_2$: $Sm_2O_3$ glasses mixed with different concentrations of $WO_3$.

In Fig. 5.4, the Raman spectra of $ZnF_2$-$WO_3$-$TeO_2$ glasses doped with $Eu^{3+}$ ions are presented. The spectrum of glass $EuW_5$ exhibited a band at about 480 $cm^{-1}$ assigned to the stretching vibrations of Te–O–Te linkages between $TeO_4$ trigonal bipyramids (tbp) and another intense band at 685 $cm^{-1}$ assigned to Te–O stretching vibration of $TeO_4$ tbp units. Yet, another significant band at about 750 $cm^{-1}$ due to $[TeO_{3+1}]^{4-}$, $[TeO_3]^{2-}$ units [114–117] is also located in the spectra. The spectrum also exhibited bands at 376 $cm^{-1}$ due to the bending vibrations of W–O–W linkages of $WO_6$ units [118]. The band due to $W–O^-$ stretchings in the $WO_4$ units is also observed at about 950 $cm^{-1}$. As the content of $WO_3$ is increased up to 15 mol%, the intensity of the bands due to $WO_6$, $[TeO_{3+1}]^{4-}$, $[TeO_3]^{2-}$ units is observed to increase gradually where as that of bands due to $TeO_4$ and $WO_4$ structural units is observed to decrease. The spectra of the other two series of the glasses exhibited similar behaviour.

Fig. 5.5 shows typical ESR spectra (recorded at room temperature) of $ZnF_2$–$TeO_2$: $Nd_2O_3$ glasses mixed with different concentrations of $WO_3$; the spectra exhibited an asymmetric signal (signal 1) identified due to$W^{5+}$ ions [Goldstein 119] at $g_\perp \sim 1.71$ and $g_\parallel \sim 1.62$ and another signal (signal 2) at higher magnetic fields which is typical for oxygen (paramagnetic $O^-$ ions) defects [120]. The intensity and half-width of these signals are observed to be maximal in the spectrum of the glass $NdW_{15}$. The ESR spectra were observed to be similar for other two series of glasses.

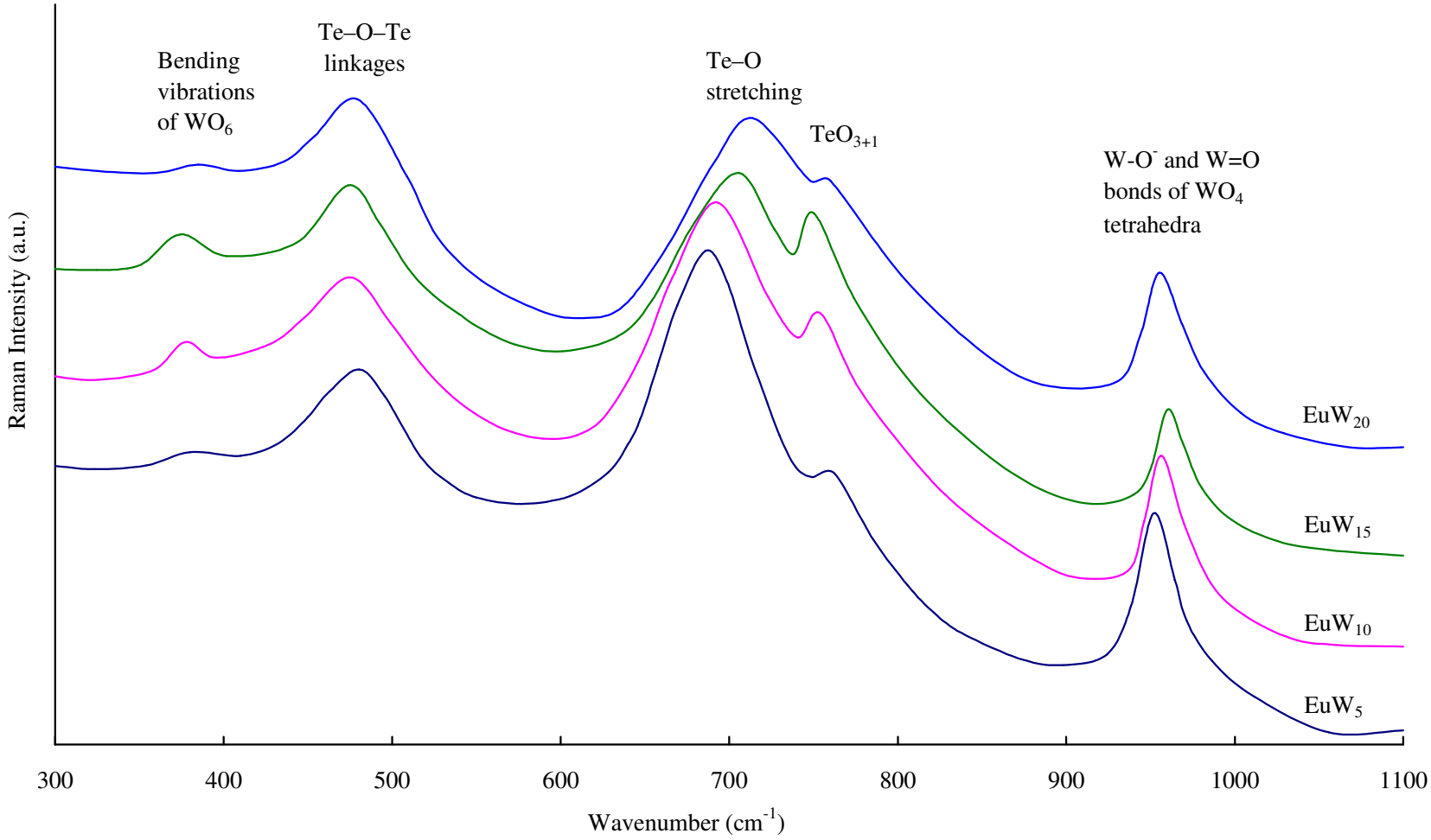


**Fig. 5.4** Raman spectra of $ZnF_2$–$WO_3$–$TeO_2$: $Eu_2O_3$ glasses mixed with different concentrations of $WO_3$.

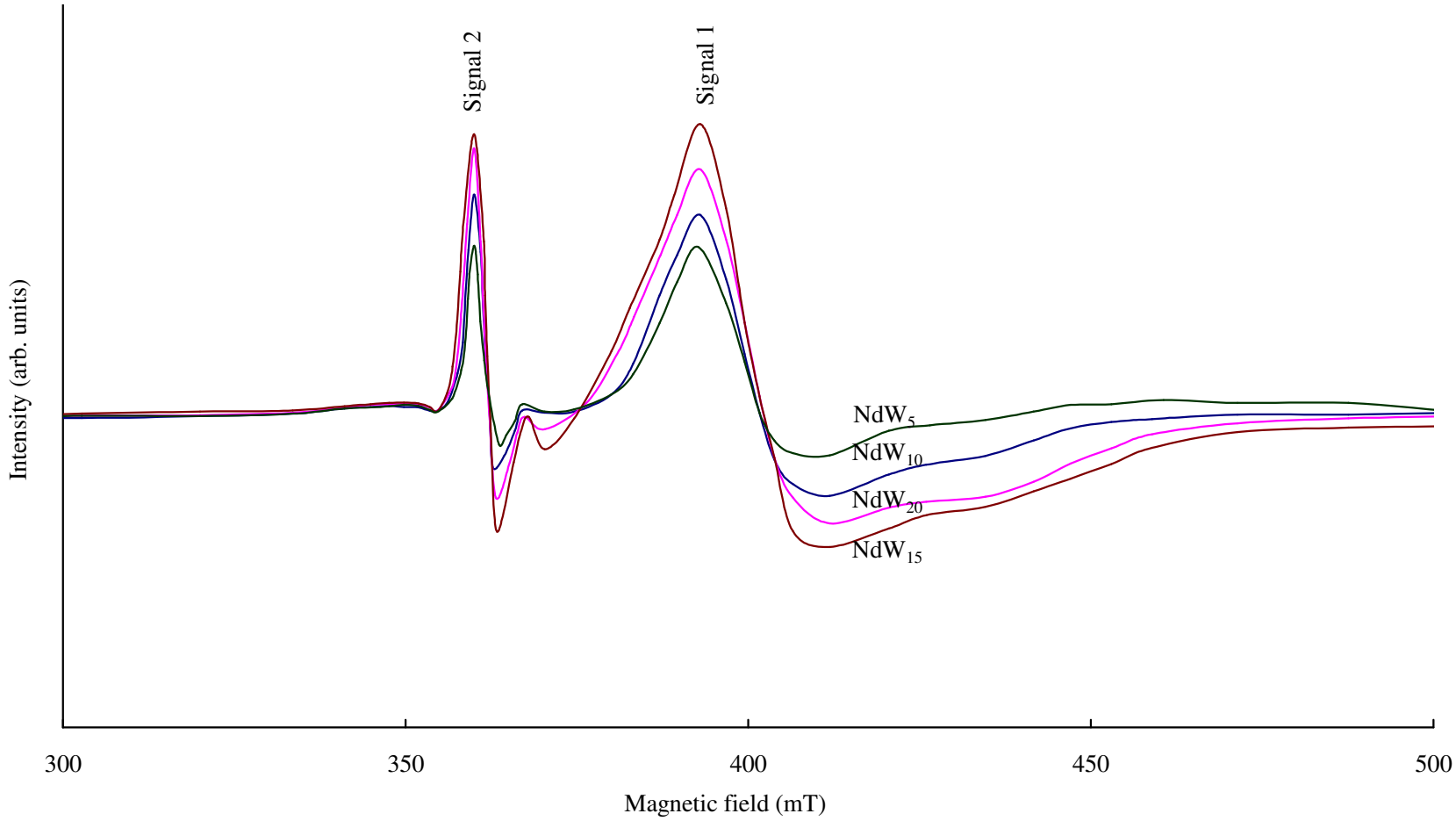


**Fig. 5.5** ESR spectra of $ZnF_2$–$WO_3$–$TeO_2$: $Eu_2O_3$ glasses mixed with different concentrations of $WO_3$.

Optical absorption spectra of the three rare earth ion doped glass samples have exhibited the bands due to the following transitions (Figs. 5.6 (a-c)).

$Nd^{3+}$: $^4I_{9/2} \rightarrow {}^2P_{1/2}$, $^2K_{15/2}+{}^2G_{9/2}+{}^2D_{3/2}+{}^4G_{11/2}$, $^4G_{9/2}$, $^2K_{13/2}+{}^4G_{7/2}$, $^4G_{5/2}+{}^2G_{7/2}$, $^2H_{11/2}$, $^4F_{9/2}$, $^4F_{7/2}+{}^4S_{3/2}$, $^4F_{5/2}$ and $^4F_{3/2}$

$Sm^{3+}$: $^6H_{5/2} \rightarrow {}^4I_{13/2}$, $^4I_{11/2}$, $^6F_{11/2}$. $^6F_{9/2}$, $^6F_{7/2}$, $^6F_{5/2}$, $^6F_{3/2}$, $^6H_{15/2}$ and $^6F_{1/2}$,

$Eu^{3+}$: $^7F_0 \rightarrow {}^5D_2$, $^7F_6$, $^7F_5$ and $^7F_1 \rightarrow {}^5D_1$

With the increase in the concentration of $WO_3$, considerable variations in the spectral peak positions and the intensity of the bands have been observed. Additionally, a weak broad band at about 1030 nm presumably due to the transitions of $W^{5+}$ ions is also observed in the spectra of these glasses with maximum intensity for $LnW_{15}$ glasses (Fig. 5.6(b)).

The experimental oscillator strengths (OS) of the absorption transitions were estimated from the spectra for all the three rare earth ion doped glasses in terms of the area under absorption peaks as described in Chapter I.

The procedure of fitting of the calculated OS to those evaluated from the experimental spectra is described in Ref. [121]. A set of matrix equations (which includes the $U^2$, $U^4$, and $U^6$ matrices, the matrices of the experimental OS and the energies of the corresponding transitions) have been solved to minimize the difference between the calculated $f_{calc}$ and observed $f_{\exp}$ OS. The quality of fitting is determined by the root mean squared deviation and presented in Tables 5.2 (a & b) for $Nd^{3+}$ and $Sm^{3+}$ doped glasses. The deviation

indicates reasonably good fitting between theory and experiment demonstrating the applicability of JO theory.

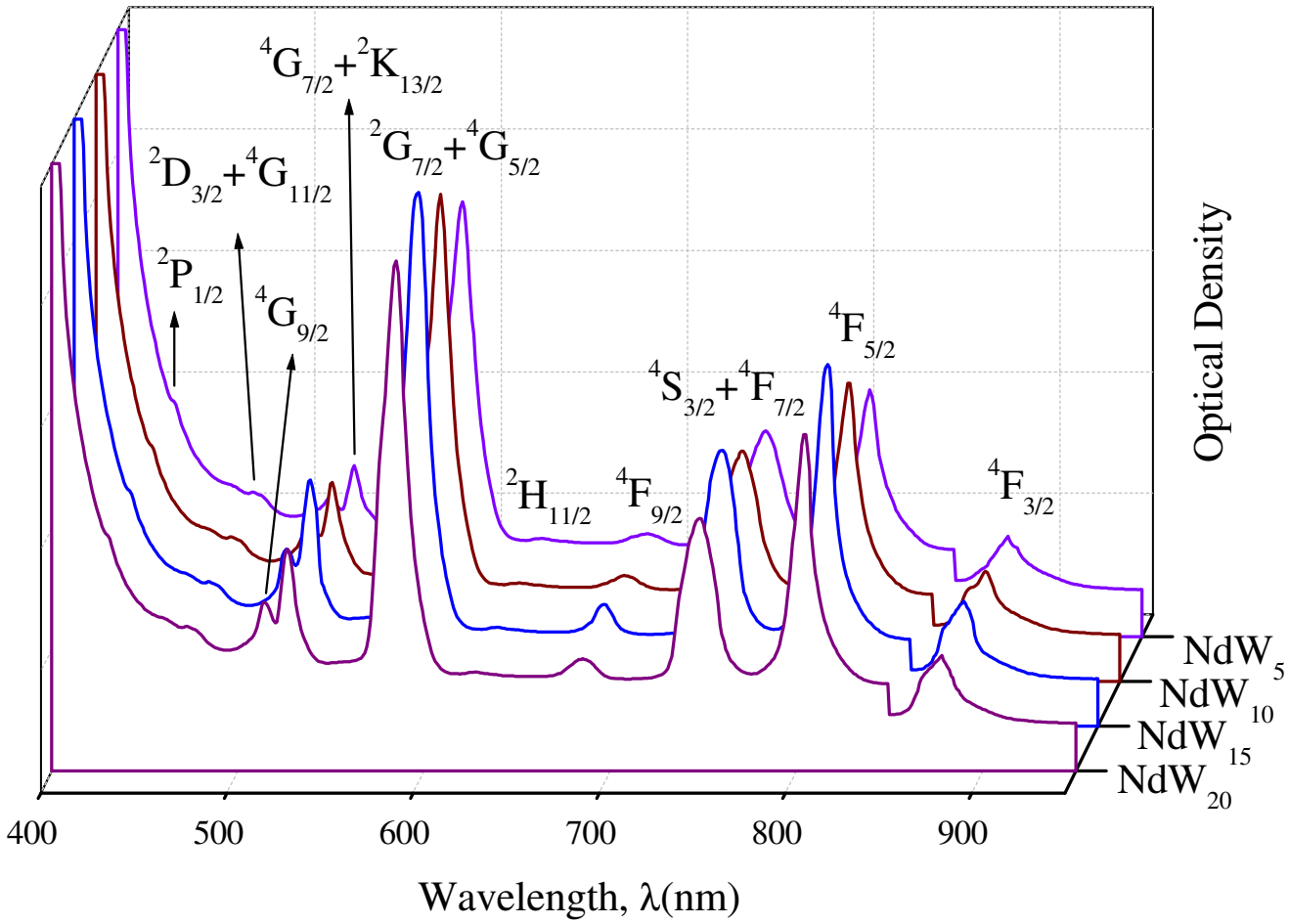


**Fig. 5.6(a)** Optical absorption spectra of $ZnF_2$–$WO_3$–$TeO_2$: $Nd_2O_3$ glasses.

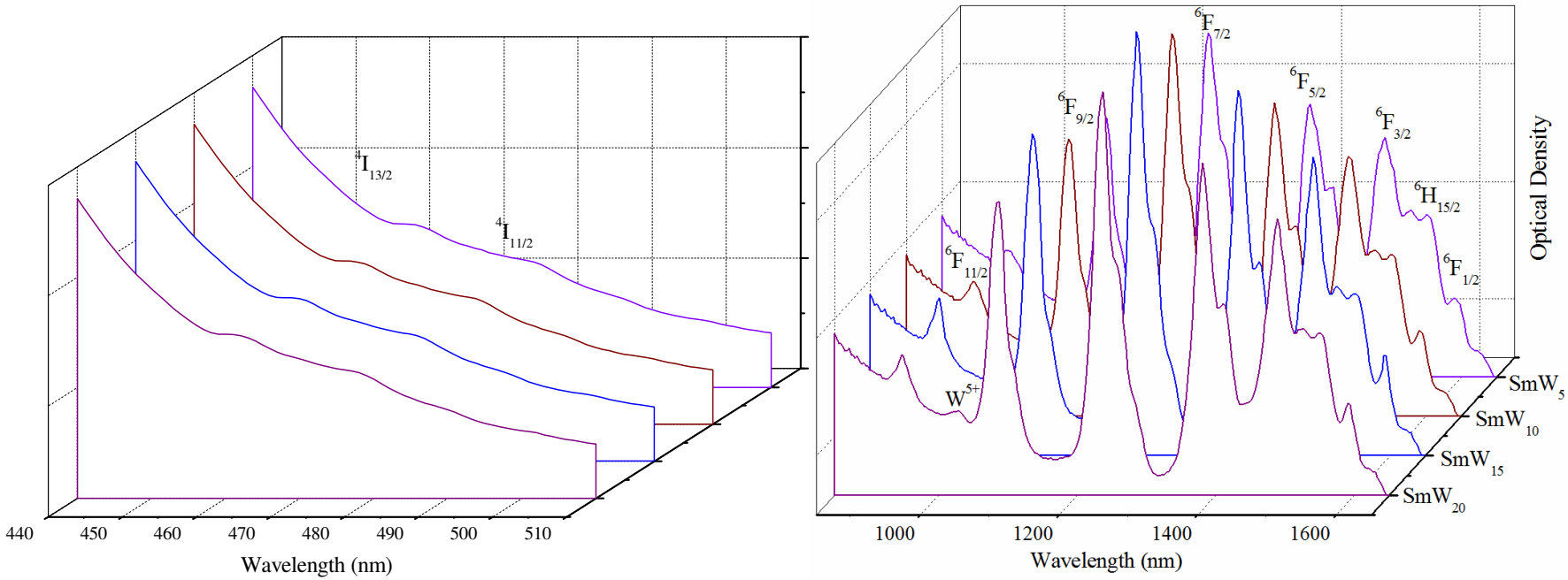


**Fig. 5.6(b)** Optical absorption spectra of $ZnF_2$–$WO_3$–$TeO_2$: $Sm_2O_3$ glasses.

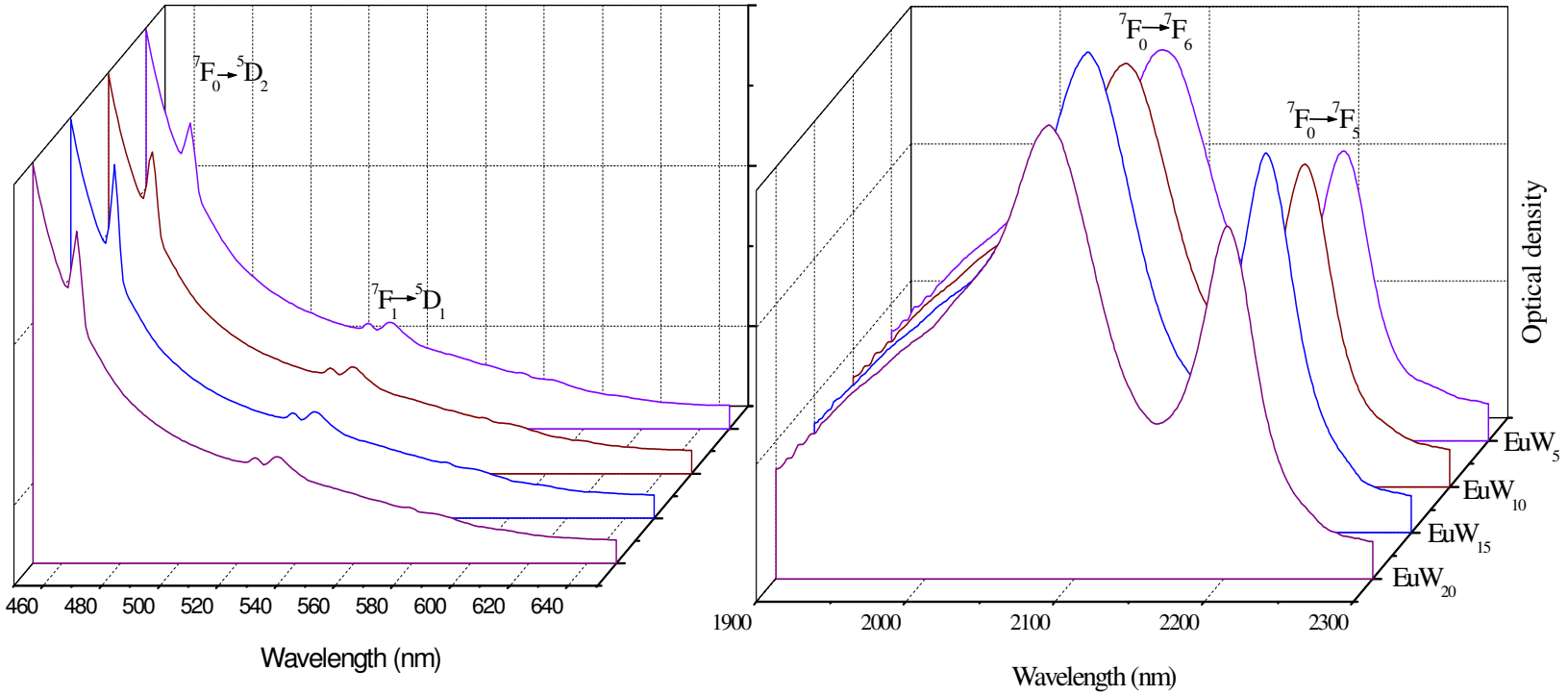


Fig. 5.6(c). Optical absorption spectra of $ZnF_2$–$WO_3$–$TeO_2$: $Eu_2O_3$ glasses.

**Table 5.2** The absorption band energies and the values of the experimental ($f_{exp}$ x$10^6$), and calculated ($f_{calc}$ x $10^6$) oscillator strengths and root mean square deviation (r.m.s.) of $Ln^{3+}$ ion in $ZnF_2$–$TeO_2$ glasses mixed with different concentrations of $WO_3$.

(a) $Nd^{3+}$ ion

| Band | $NdW_5$ | | | $NdW_{10}$ | | | $NdW_{15}$ | | | $NdW_{20}$ | | |
|---|---|---|---|---|---|---|---|---|---|---|---|---|
| | $\nu$ ($cm^{-1}$) | $f_{exp}$ | $f_{calc}$ | $\nu$ ($cm^{-1}$) | $f_{exp}$ | $f_{calc}$ | $\nu$ ($cm^{-1}$) | $f_{exp}$ | $f_{calc}$ | $\nu$ ($cm^{-1}$) | $f_{exp}$ | $f_{calc}$ |
| $^2K_{15/2}$+$^2G_{9/2}$+ $^2D_{3/2}$+$^4G_{11/2}$ | 21148.8 | 4.135 | 4.265 | 21079.1 | 4.203 | 4.546 | 21034.5 | 4.789 | 4.842 | 21057.1 | 4.468 | 4.751 |
| $^4G_{9/2}$ | 19652.5 | 4.336 | 4.591 | 19558.2 | 4.035 | 4.947 | 19529.3 | 5.024 | 4.984 | 19533.2 | 4.598 | 4.487 |
| $^2K_{13/2}$+ $^4G_{7/2}$ | 18958.1 | 11.157 | 14.568 | 18918.9 | 10.362 | 16.187 | 18885.7 | 16.425 | 16.985 | 18905.7 | 14.856 | 17.054 |
| $^4G_{5/2}$ + $^2G_{7/2}$ | 17128 | 82.045 | 82.926 | 17101.5 | 84.554 | 84.110 | 17094.6 | 86.754 | 86.592 | 17099.9 | 85.492 | 85.843 |
| $^2H_{11/2}$ | 15860.4 | 0.103 | 0.210 | 15836.6 | 0.114 | 0.538 | 15796.5 | 0.213 | 0.305 | 15820.3 | 0.208 | 0.254 |
| $^4F_{9/2}$ | 14661.6 | 3.059 | 2.843 | 14607.8 | 3.438 | 2.341 | 14537.0 | 3.925 | 2.982 | 14577.3 | 3.834 | 3.715 |
| $^4F_{7/2}$ + $^4S_{3/2}$ | 13426.4 | 22.583 | 22.847 | 13385.9 | 23.996 | 26.025 | 13355.1 | 25.648 | 26.285 | 13372.6 | 25.317 | 25.745 |
| $^4F_{5/2}$ | 12478.2 | 24.678 | 23.148 | 12423.6 | 25.776 | 20.243 | 12367.1 | 26.084 | 25.892 | 12400.8 | 26.824 | 26.158 |
| $^4F_{3/2}$ | 11415.5 | 7.308 | 7.273 | 11369.3 | 7.739 | 7.544 | 11350.2 | 8.124 | 8.087 | 11361.1 | 8.182 | 7.806 |
| r.m.s | 1.289 | | | 0.763 | | | 0.433 | | | 0.805 | | |

(b) $Sm^{3+}$ ion

| Band | $SmW_5$ | | | $SmW_{10}$ | | | $SmW_{15}$ | | | $SmW_{20}$ | | |
|---|---|---|---|---|---|---|---|---|---|---|---|---|
| | $\nu$ ($cm^{-1}$) | $f_{exp}$ | $f_{calc}$ | $\nu$ ($cm^{-1}$) | $f_{exp}$ | $f_{calc}$ | $\nu$ ($cm^{-1}$) | $f_{exp}$ | $f_{calc}$ | $\nu$ ($cm^{-1}$) | $f_{exp}$ | $f_{calc}$ |
| $^6F_{11/2}$ | 10565 | 0.785 | 0.915 | 10541 | 0.801 | 1.031 | 10523 | 1.145 | 1.031 | 10530 | 0.953 | 1.053 |
| $^6F_{9/2}$ | 9220 | 6.026 | 6.157 | 9195 | 5.946 | 6.327 | 9181.1 | 6.283 | 6.327 | 9185 | 6.276 | 6.624 |
| $^6F_{7/2}$ | 8056 | 8.246 | 8.734 | 8043 | 9.658 | 9.281 | 8030.8 | 10.295 | 9.281 | 8035 | 10.163 | 10.053 |
| $^6F_{5/2}$ | 7213 | 4.907 | 5.017 | 7209 | 5.360 | 5.113 | 7197.9 | 5.452 | 5.692 | 7202 | 5.386 | 5.475 |
| $^6F_{3/2}$ | 6744 | 1.248 | 1.833 | 6732 | 1.548 | 2.488 | 6721.3 | 2.205 | 2.819 | 6726 | 1.982 | 2.108 |
| $^6F_{1/2}$ $+^6H_{15/2}$ | 6445 | 1.148 | 0.751 | 6431 | 1.008 | 0.328 | 6419.3 | 1.352 | 1.407 | 6425 | 1.342 | 1.291 |
| | r.m.s | 0.361 | | | 3.446 | | | 0.497 | | | 0.168 | |

The summary of the JO parameters $\Omega_\lambda$ for the rare earth ion ($Nd^{3+}$ and $Sm^{3+}$) doped $ZnF_2$–$WO_3$–$TeO_2$ glasses is presented in Tables 5.3 (a & b). However, for $Eu^{3+}$ doped glasses, Judd-Ofelt intensity parameters have been calculated directly from the emission spectra since the well resolved absorption bands could not be observed in the visible region.

The bonding parameter ($\delta$), defined as [122, 123]

$$\delta = [(1-\overline{\beta}) / \overline{\beta}] \times 100, \qquad (5.1)$$

is computed for all the three series of glasses. In Eq. (2), $\overline{\beta} = \sum_{1N} \beta / N$ and $\beta$ (the nephelauxetic ratio) = $\nu_c/\nu_a$. $\nu_c$ and $\nu_a$ are the energies in $cm^{-1}$ of the corresponding transitions in the complex and aquo-ion respectively and N refers to the number of levels used to compute $\overline{\beta}$ values. The computation shows a slight decrease of $\delta$ value with the increase of $WO_3$ up to 15 mol% (Table 5.3).

**Table 5.3** Summary of the JO parameters $\Omega_\lambda$ for the rare earth ion doped $ZnF_2$–$WO_3$ –$TeO_2$ glasses.

(a) $Nd^{3+}$ doped glasses

| Glass | $\Omega_2$ | $\Omega_4$ | $\Omega_6$ | $\Omega_4/\Omega_6$ | $\delta$ |
|---|---|---|---|---|---|
| $NdW_5$ | 26.85 | 17.69 | 21.67 | 0.82 | 0.876 |
| $NdW_{10}$ | 24.55 | 15.07 | 19.23 | 0.78 | 0.824 |
| $NdW_{15}$ | 20.63 | 13.56 | 18.83 | 0.72 | 0.792 |
| $NdW_{20}$ | 22.45 | 14.10 | 17.72 | 0.80 | 0.807 |

(b)$Sm^{3+}$ doped glasses

| Glass | $\Omega_2$ | $\Omega_4$ | $\Omega_6$ | $\Omega_4/\Omega_6$ | $\delta$ |
|---|---|---|---|---|---|
| $SmW_5$ | 0.96 | 15.47 | 9.62 | 1.61 | -0.0916 |
| $SmW_{10}$ | 0.91 | 10.17 | 7.66 | 1.33 | -0.0959 |
| $SmW_{15}$ | 0.82 | 9.15 | 7.15 | 1.28 | -0.1060 |
| $SmW_{20}$ | 0.90 | 9.65 | 7.28 | 1.32 | -0.0972 |

The luminescence spectra of all the three series of glasses recorded at room temperature in the visible and NIR regions are shown in Fig. 5.7 (a), (b) and (c). The spectra exhibited the following prominent emission bands:

$Nd^{3+}(\lambda_{exc}= 878\ nm) : {}^4F_{3/2} \rightarrow {}^4I_{9/2}, {}^4I_{11/2}, \mathbf{{}^4I_{13/2}}$

$Sm^{3+}(\lambda_{exc}= 462\ nm) : {}^4G_{5/2} \rightarrow {}^6H_{5/2}, \mathbf{{}^6H_{7/2}}, {}^6H_{9/2}$

$Eu^{3+}(\lambda_{exc}= 465\ nm) : {}^5D_0 \rightarrow {}^7F_0, {}^7F_1, \mathbf{{}^7F_2}, {}^7F_3, {}^7F_4$

It is noticed that with increase in the content of $WO_3$ up to 15 mol%, the intensity of the three principal bands viz., ${}^4F_{3/2} \rightarrow {}^4I_{13/2}$ ($Nd^{3+}$), ${}^4G_{5/2} \rightarrow {}^6H_{7/2}$ ($Sm^{3+}$), ${}^5D_0 \rightarrow {}^7F_2$ ($Eu^{3+}$) is observed to increase.

The energy level diagrams containing observed absorption and emission transitions of $Nd^{3+}$, $Sm^{3+}$ and $Eu^{3+}$ ions for one of the glasses (glass containing 10 mol% $WO_3$) in each series are shown in Fig. 5.8.

Using JO intensity parameters, the radiative transition probability from the excited state $\langle f^N[\gamma,S,L]J|$ to the lower state $|f^N[\gamma',S',L']J'\rangle$ , total radiative probability, the radiative life time $\tau$ of an excited energy level and the

branching ratio $\beta_{JJ'}$ are evaluated using the standard equations reported in Chapter I.

The details of emission parameters for the glasses mixed with 10 mol% of $WO_3$ for all the three rare earth doped glasses are presented in Tables 5.4 (a, b and c) and the summary of these data for the three principal levels in Table 5.5. Since the matrix elements of the unit tensor operators for the $^5D_0 \rightarrow {}^7F_3$ transition for $Eu^{3+}$ ion are zero, estimation of the radiative transition probability could not be possible.

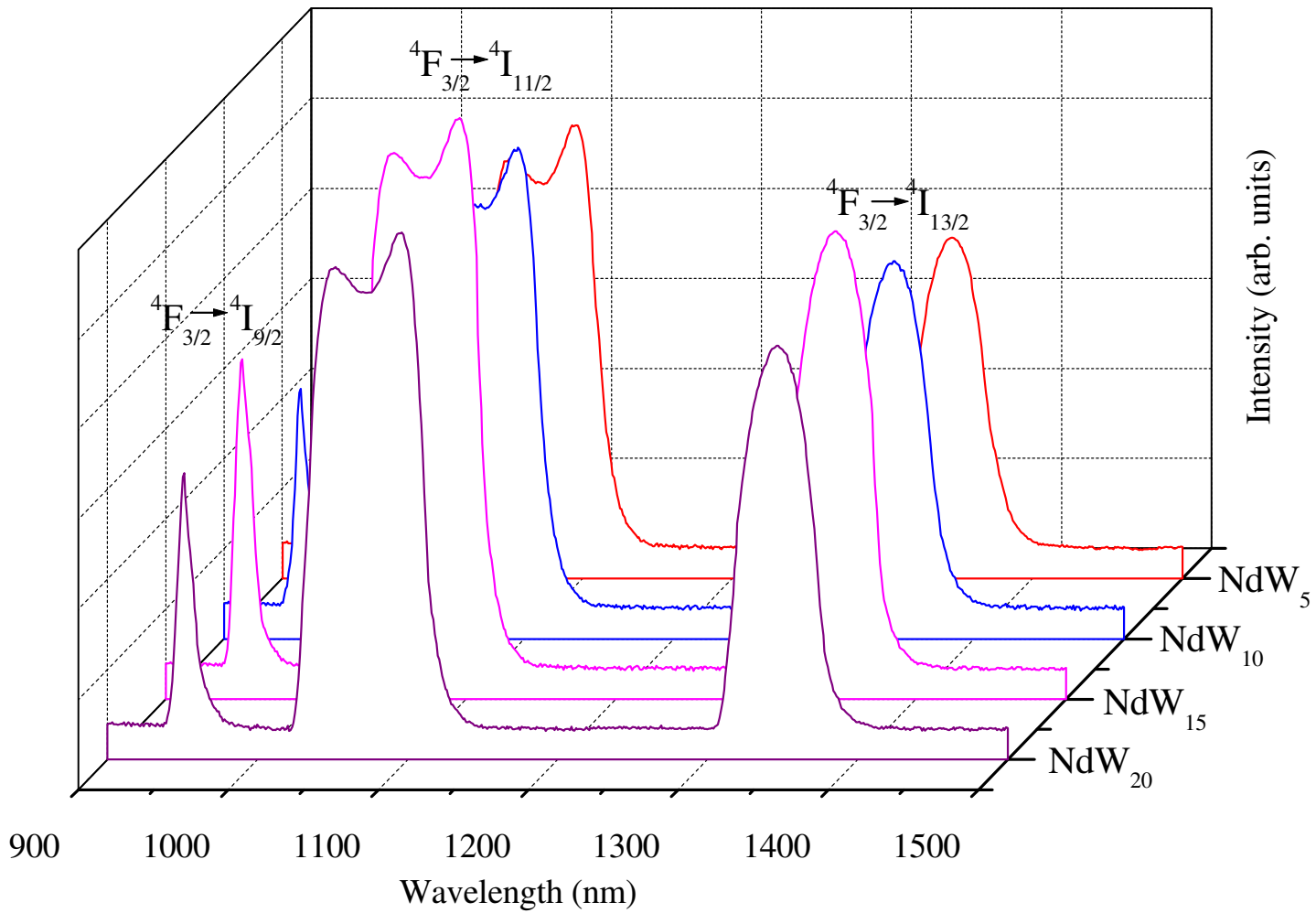


**Fig. 5.7(a)** Photoluminescence spectra of $ZnF_2$–$WO_3$–$TeO_2$: $Nd_2O_3$ glasses recorded at room temperature ($\lambda_{exc}$ = 878 nm).

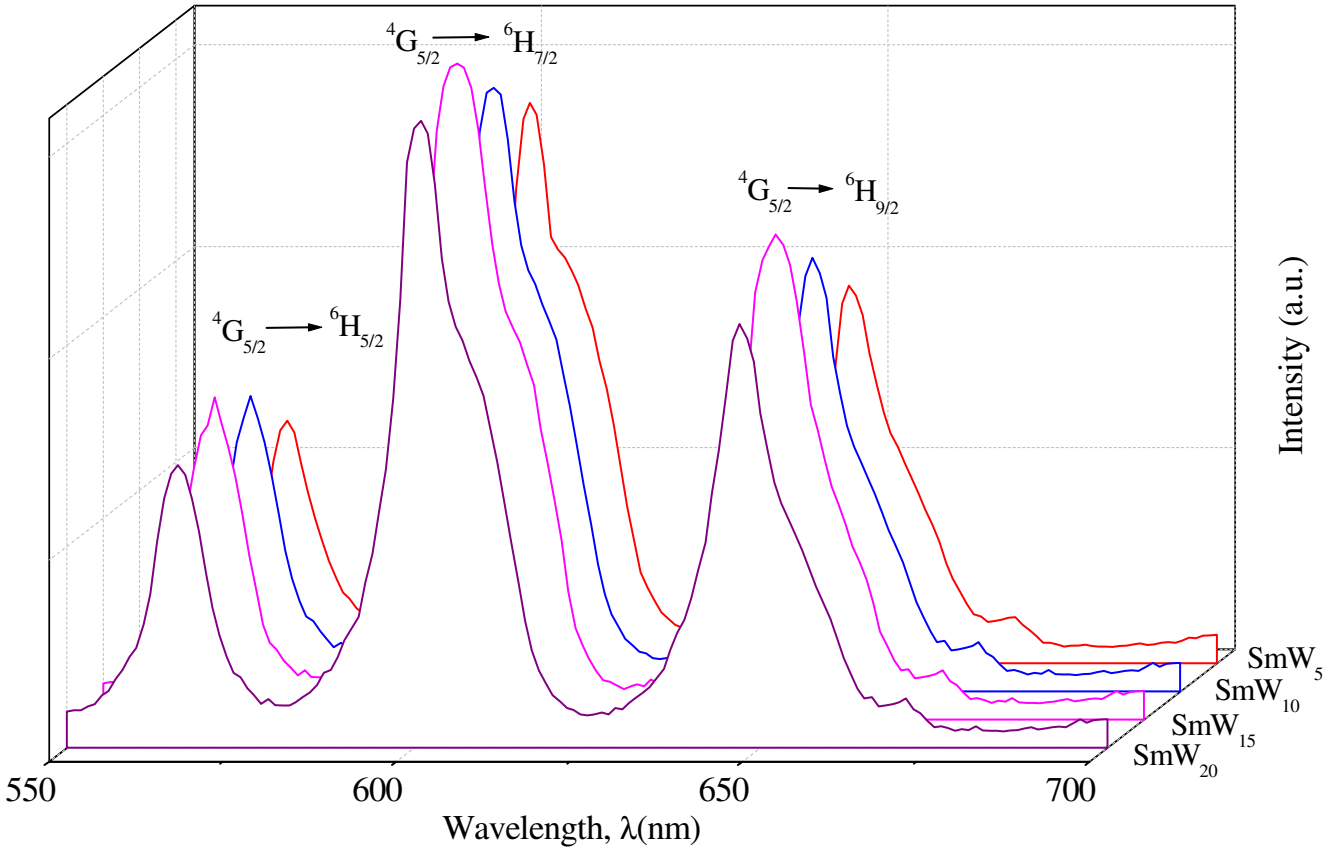


**Fig. 5.7(b)** Photoluminescence spectra of $ZnF_2$–$WO_3$–$TeO_2$: $Sm_2O_3$ glasses recorded at room temperature ($\lambda_{exc}$ = 462 nm).

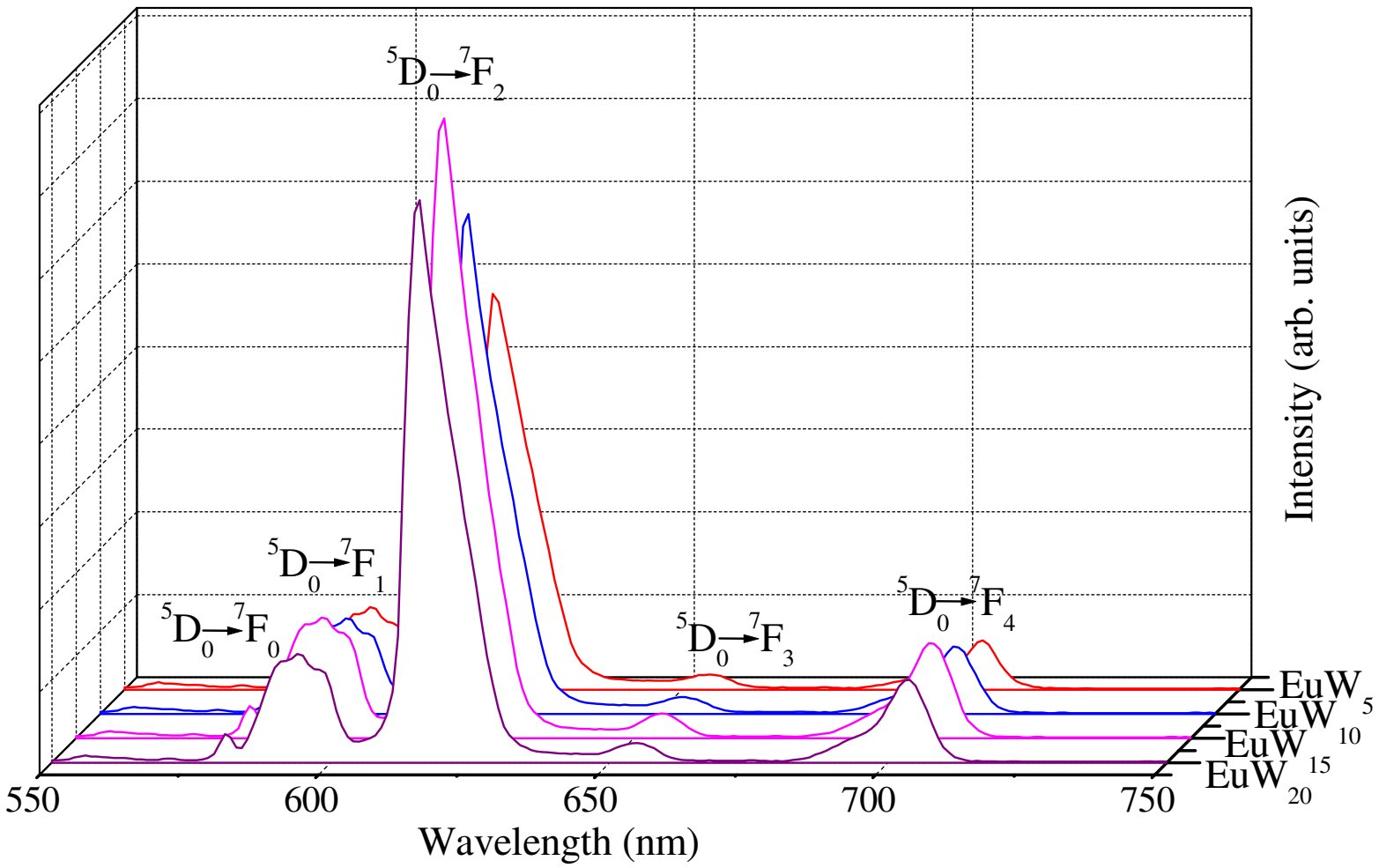


**Fig. 5.7(c)** Photoluminescence spectra of $ZnF_2$–$WO_3$–$TeO_2$: $Eu_2O_3$ glasses recorded at room temperature ($\lambda_{exc}$ = 465 nm).

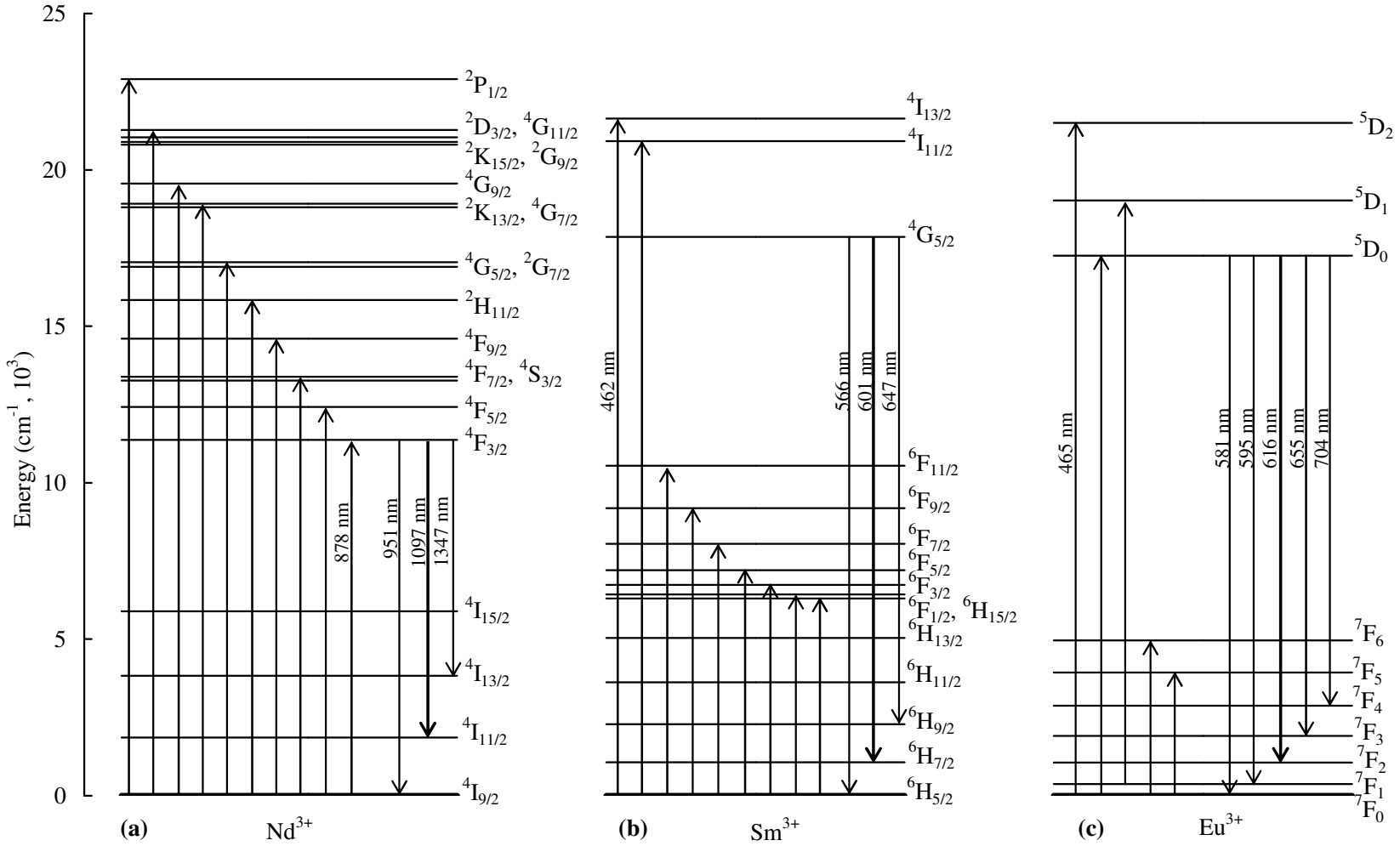


**Fig. 5.8** The energy level diagrams containing observed absorption and emission transitions of $Nd^{3+}$, $Sm^{3+}$ and $Eu^{3+}$ ions in $ZnF_2$–$TeO_2$ glasses mixed with 10 mol % of $WO_3$.

**Table 5.4(a)** Radiative parameters of $Nd^{3+}$ doped $ZnF_2$–$TeO_2$ glasses mixed with 10 mol% of $WO_3$.

| Initial state and calculated radiative lifetime | Final state | ν, $cm^{-1}$ | Radiative probability $A$ ($s^{-1}$) | Branching ratio β% |
|---|---|---|---|---|
| $^2K_{15/2} + {}^2G_{9/2} + {}^2D_{3/2} + {}^4G_{11/2}$ $\tau = 12$ μs | $^4I_{9/2}$ | 21079 | 3635.0 | 44.0 |
| | $^4I_{11/2}$ | 19222 | 9268.6 | 11.22 |
| | $^4I_{13/2}$ | 17243 | 22030 | 26.67 |
| | $^4I_{15/2}$ | 15183 | 37195 | 45.03 |
| | $^4F_{3/2}$ | 9710.1 | 591.73 | 0.72 |
| | $^2H_{9/2}$ | 9028.1 | 3400.5 | 4.12 |
| | $^4F_{5/2}$ | 8655.5 | 874.32 | 1.06 |
| | $^4F_{7/2}+{}^4S_{3/2}$ | 7693.2 | 1865 | 2.25 |
| | $^4F_{9/2}$ | 6472.1 | 2033.7 | 2.46 |
| | $^2H_{11/2}$ | 5242.5 | 1492.8 | 1.81 |
| | $^4G_{5/2}+{}^2G_{7/2}$ | 3977.6 | 150.2 | 0.18 |
| | $^2K_{13/2}$ | 2160.2 | 25.664 | 0.03 |
| | $+{}^4G_{7/2}$ | | 24.804 | 0.03 |
| | $^4G_{9/2}$ | 1520.9 | 13.041 | 0.02 |
| | | | $\sum_{J'} A_{JJ'}$ =82601 | |
| $^4G_{9/2}$ $\tau = 22$ μs | $^4I_{9/2}$ | 19558 | 2847.4 | 6.16 |
| | $^4I_{11/2}$ | 17701 | 11748 | 25.41 |
| | $^4I_{13/2}$ | 15722 | 25402 | 54.94 |
| | $^4I_{15/2}$ | 13662 | 3809.6 | 8.24 |
| | $^4F_{3/2}$ | 8189.2 | 444.13 | 0.96 |
| | $^2H_{9/2}$ | 7507.2 | 291.85 | 0.63 |
| | $^4F_{5/2}$ | 7134.6 | 499.24 | 1.08 |
| | $^4F_{7/2}+{}^4S_{3/2}$ | 6172.3 | 938.99 | 2.0 |
| | $^4F_{9/2}$ | 4951.2 | 163.04 | 0.35 |
| | $^2H_{11/2}$ | 3721.6 | 55.32 | 0.12 |
| | $^4G_{5/2}+{}^2G_{7/2}$ | 2456.7 | 33.9 | 0.08 |
| | $^2K_{13/2}$ $+{}^4G_{7/2}$ | 639.30 | 0.51 | 0.0 |
| | | | $\sum_{J'} A_{JJ'}$ =46234 | |

| | | | | |
|---|---|---|---|---|
| $^2K_{13/2}+{}^4G_{7/2}$ $\tau = 23$ μs | $^4I_{9/2}$ | 18919 | 10293 | 23.56 |
| | $^4I_{11/2}$ | 17062 | 24692 | 56.51 |
| | $^4I_{13/2}$ | 15083 | 4580.0 | 10.48 |
| | $^4I_{15/2}$ | 13023 | 341.93 | 0.78 |
| | $^4F_{3/2}$ | 7549.9 | 428.65 | 0.98 |
| | $^2H_{9/2}$ | 6867.9 | 2137.2 | 4.89 |
| | $^4F_{5/2}$ | 6495.3 | 639.74 | 1.46 |
| | $^4F_{7/2}+{}^4S_{3/2}$ | 5533.0 | 417.86 | 0.95 |
| | $^4F_{9/2}$ | 4311.9 | 81.23 | 0.19 |
| | $^2H_{11/2}$ | 3082.3 | 62.297 | 0.14 |
| | $^4G_{5/2}+{}^2G_{7/2}$ | 1817.4 | 21.362 | 0.0005 |
| | | | $\sum_{J'} A_{JJ'}$ =43695 | |

| | | | | |
|---|---|---|---|---|
| $^4G_{5/2}+{}^2G_{7/2}$ $\tau =$ 12 μs | $^4I_{9/2}$ | 17102 | 59463 | 69.01 |
| | $^4I_{11/2}$ | 15244 | 21345 | 24.77 |
| | $^4I_{13/2}$ | 13266 | 2495.6 | 02.90 |
| | $^4I_{15/2}$ | 11206 | 874.04 | 01.01 |
| | $^4F_{3/2}$ | 5732.5 | 989.07 | 01.15 |
| | $^2H_{9/2}$ | 5050.5 | 185.17 | 00.21 |
| | $^4F_{5/2}$ | 4677.9 | 540.89 | 00.63 |
| | $^4F_{7/2}+{}^4S_{3/2}$ | 3715.6 | 231.51 | 00.27 |
| | $^4F_{9/2}$ | 2494.5 | 40.75 | 00.05 |
| | $^2H_{11/2}$ | 1264.9 | 4.034 | 0.0 |
| | | | $\sum_{J'} A_{JJ'}$ =86169 | |

| | | | | |
|---|---|---|---|---|
| $^2H_{11/2}$ $\tau = 794$ μs | $^4I_{9/2}$ | 15837 | 169.25 | 13.43 |
| | $^4I_{11/2}$ | 13980 | 173.54 | 13.77 |
| | $^4I_{13/2}$ | 12001 | 123.87 | 09.83 |
| | $^4I_{15/2}$ | 9940.6 | 710.00 | 56.35 |
| | $^4F_{3/2}$ | 4467.6 | 2.4674 | 00.20 |
| | $^2H_{9/2}$ | 3785.6 | 63.68 | 05.05 |
| | $^4F_{5/2}$ | 3413.0 | 3.46 | 00.27 |
| | $^4F_{7/2}$ | 2450.7 | 11.73 | 00.93 |
| | $^4F_{9/2}$ | 1229.6 | 1.11 | 00.09 |
| | | | $\sum_{J'} A_{JJ'}$ =1260 | |

| | | | | |
|---|---|---|---|---|
| $^4F_{9/2}$ $\tau = 95\ \mu s$ | $^4I_{9/2}$ | 14607 | 751.49 | 07.15 |
| | $^4I_{11/2}$ | 12750 | 3524.4 | 33.53 |
| | $^4I_{13/2}$ | 10771 | 3701.1 | 35.21 |
| | $^4I_{15/2}$ | 8711.0 | 2502.1 | 23.80 |
| | $^4F_{3/2}$ | 3238.0 | 17.299 | 00.16 |
| | $^2H_{9/2}$ | 2556.0 | 4.8326 | 00.05 |
| | $^4F_{5/2}$ | 2183.4 | 7.2591 | 00.07 |
| | $^4F_{7/2}+^4S_{3/2}$ | 1221.1 | 2.09 | 0.02 |
| | | | $\sum_{J'} A_{JJ'} = 10511$ | |

| | | | | |
|---|---|---|---|---|
| $^4F_{7/2}+^4S_{3/2}$ $\tau = 38\ \mu s$ | $^4I_{9/2}$ | 13386 | 11732 | 44.44 |
| | $^4I_{11/2}$ | 11529 | 7390.8 | 28.00 |
| | $^4I_{13/2}$ | 9549.9 | 4178.9 | 15.83 |
| | $^4I_{15/2}$ | 7489.9 | 3090.6 | 11.71 |
| | $^4F_{3/2}$ | 2016.9 | 3.10 | 0.01 |
| | $^2H_{9/2}$ | 1334.9 | 0.52 | 0.0 |
| | $^4F_{5/2}$ | 962.30 | 0.90 | 0.0 |
| | | | $\sum_{J'} A_{JJ'} = 26396$ | |

| | | | | |
|---|---|---|---|---|
| $^4F_{5/2}$ $\tau = 83\ \mu s$ | $^4I_{9/2}$ | 12424 | 7835.7 | 64.69 |
| | $^4I_{11/2}$ | 10567 | 1410.1 | 11.64 |
| | $^4I_{13/2}$ | 8587.6 | 2415.8 | 19.95 |
| | $^4I_{15/2}$ | 6527.6 | 448.90 | 3.71 |
| | $^4F_{3/2}$ | 1054.6 | 1.16 | 0.0 |
| | $^2H_{9/2}$ | 372.60 | 0.012 | 0.0 |
| | | | $\sum_{J'} A_{JJ'} = 12112$ | |

| | | | | |
|---|---|---|---|---|
| $^4F_{3/2}$ $\tau = 107\ \mu s$ | $^4I_{9/2}$ | 11369 | 3668.2 | 39.25 |
| | $^4I_{11/2}$ | 9512.0 | 4672.0 | 49.99 |
| | $^4I_{13/2}$ | 7533.0 | 959.81 | 10.27 |
| | $^4I_{15/2}$ | 5473.0 | 46.065 | 0.49 |
| | | | $\sum_{J'} A_{JJ'} = 9346$ | |

**Table 5.4(b)** Radiative parameters of $Sm^{3+}$ doped $ZnF_2$–$TeO_2$ glasses mixed with 10 mol% of $WO_3$.

| Initial state and calculated radiative lifetime | Final state | ν, $cm^{-1}$ | Radiative probability $A$ ($s^{-1}$) | Branching ratio β% |
|---|---|---|---|---|
| $^4G_{5/2}$ τ = 2.2 ms | $^6H_{5/2}$ | 17700 | 13.86 | 3.09 |
| | $^6H_{7/2}$ | 16669 | 238.02 | 53.13 |
| | $^6H_{9/2}$ | 15465 | 112.65 | 25.15 |
| | $^6H_{11/2}$ | 14142 | 59.65 | 13.31 |
| | $^6H_{13/2}$ | 12741 | 7.62 | 1.70 |
| | $^6F_{1/2}$ + $^6H_{15/2}$ | 11269 | 0.76 | 0.06 |
| | $^6F_{3/2}$ | 10968 | 0.73 | 0.10 |
| | $^6F_{5/2}$ | 10491 | 8.22 | 0.16 |
| | $^6F_{7/2}$ | 9657.0 | 4.8100 | 1.83 |
| | $^6F_{9/2}$ | 8505.0 | 1.25 | 1.07 |
| | $^6F_{11/2}$ | 7159 | 0.44 | 0.28 |
| | | | $\sum_{J'} A_{JJ'}$ =448 | |

**Table 5.4(c)** Radiative parameters of $Eu^{3+}$ doped $ZnF_2$–$TeO_2$ glasses mixed with 10 mol% of $WO_3$.

| Initial state and calculated radiative lifetime | Final state | ν, $cm^{-1}$ | Radiative probability $A$ ($s^{-1}$) | Branching ratio β% |
|---|---|---|---|---|
| $^5D_0$ τ = 2.9 ms | $^7F_1$ | 16806.7 | 49 | 14.5 |
| | $^7F_2$ | 16233.8 | 251 | 73.7 |
| | $^7F_4$ | 14204.6 | 40 | 11.8 |
| | | | $\sum_{J'} A_{JJ'}$ =340 | |

**Table 5.5** A comparison of radiative lifetimes (τ) and quantum efficiencies (η) for the principal transitions in $ZnF_2$–$WO_3$–$TeO_2$:$Ln^{3+}$ glasses.

| $WO_3$ conc. (mol %) | $Nd^{3+}$ doped glasses ($^4F_{3/2}$ level) | | | $Sm^{3+}$ doped glasses ($^4G_{5/2}$ level) | | | $Eu^{3+}$ doped glasses ($^5D_0$ level) | | |
|---|---|---|---|---|---|---|---|---|---|
| | ($\tau_m$) μs | ($\tau_c$) μs | (η%) | ($\tau_m$) ms | (τ) ms | (η%) | ($\tau_m$) ms | (τ) ms | (η%) |
| 5 | 65.14 | 95 | 68.57 | 0.98 | 1.60 | 61.25 | 1.04 | 2.50 | 41.60 |
| 10 | 82.52 | 107 | 77.12 | 1.48 | 2.20 | 67.27 | 1.27 | 2.90 | 43.79 |
| 15 | 102.06 | 116 | 87.98 | 1.93 | 2.72 | 70.96 | 1.69 | 3.25 | 52.0 |
| 20 | 91.20 | 109 | 83.67 | 1.80 | 2.61 | 68.97 | 1.39 | 2.85 | 48.77 |

## 5.4 Discussion

$WO_3$ belongs to the intermediate class of glass forming oxides. It is an incipient glass network former, normally tungsten ion exists in $W^{6+}$ state and participates in glass network with $WO_4$ and $WO_6$ structural units and may alternate with tellurite structural units and form the linkages of the type Te–O–W as mentioned earlier [124, 125]. Tungsten ions also exist in stable $W^{5+}$ state, form $W^{5+}O_3$ complexes and occupy octahedral positions with distortions due to the Jahn-Teller effect [126] and decrease the long range ordering in the glass network. Brenier and Kityk have demonstrated that such a decease in the long range orders leads to a substantial widening of the emission peaks of rare earth ions present in the glass matrix [127]. A weak kink (at 1030 nm Fig. 5.6) observed in the optical absorption spectra of with the highest intensity in the glasses $LnW_{15}$ is identified due to $d_{xy} \rightarrow d_{x^2-y^2}$ transition of $W^{5+}$ ions indicating conversion of a part of tungsten ions into $W^{5+}$ state.

The observed increase in the half width and the intensity of the ESR signal with the concentration of $WO_3$ up to 15 mol% obviously suggests the gradual hike in the concentration of $W^{5+}$ ions in the glass matrix. The value of g factor observed in the range $1.65 < g_{\perp} < 1.75$ and $1.55 < g_{\parallel} < 1.65$ indicate that $W^{5+}$ ions present in axially distorted octahedral positions with a short W-O bond and an opposite long W–O bond along the symmetry axis of oxygen ions [125]. Additionally the difference between $g_{\parallel}$ and $g_{\perp}$ (anisotropy factor) changes is different for different for rare earth ion doped glasses in the glass network; this observation indicates that $W^{5+}$ octahedron experiences different structural changes for different rare earth ion doped glasses.

Overall, there is a gradual increase in structural depolymerization in the glasses with increase in the content of $WO_3$ up to 15 mol%. This result is also consistent with the variations in $T_g$ and $T_c$–$T_g$ values observed in the DSC studies. With increase in the concentration of $WO_3$ up to 15 mol%, the glass transition temperature $T_g$ and the glass forming ability parameter have exhibited a decreasing trend. Such trend indicates the lessening of augmented cross–link density of various structural groups and closeness of packing.

Yet, another support for this argument can also be obtained from IR and Raman spectra. In these spectra it is observed that the symmetrical vibrational frequencies of $\nu^{s}_{ax}$–$TeO_2$ bonds of $TeO_4$ groups in the IR spectra are spectrally shifted towards higher frequencies with decreasing intensity as the

concentration of $WO_3$ is increased up to 15 mol%. The intensity of the bands due to $WO_6$ structural units is observed to increase at the expense of the band due to $WO_4$ structural units. These observations clearly indicate that there is an increasing degree of disorder owing due to increasing content of modifying $W^{5+}$ ions.

The $W^{5+}$ ions are expected to occupy only interstitial positions and act as modifiers since the ratio of cation-oxygen radii is 0.45 for $W^{5+}$ ion, which is far from the value of 0.19 possessed by an ion to occupy tetrahedral or substitutional sites [128]. These ions enter the glass network by breaking up W–O–Te and Te–O–Te bonds and introduce: (i) the stable $Te–O^-$ and (ii) unstable $Te–O^-$ bonds which will later be modified to $Te–O^-$ (or simply $TeO_{3+1}$) owing to the contraction of one $Te\text{-}O^-$ and the elongation of another $Te–O^-$ bond as illustrated in Fig. 5.9. With increasing $WO_3$ content (up to 15 mol%), cleavage of continuous network leads to an increase in the fraction of $TeO_{3+1}$ polyhedra. Further, the elongation of Te–O bond of $TeO_{3+1}$ and its cleavage finally lead to the formation of trigonal prismatic $TeO_3$ units. Thus in addition to Te–O–Te, W–O–Te linkages, $WO_4$ and $WO_6$ units, the structure of the studied glass network consists of $TeO_{3+1}$ and $TeO_3$, free $Zn^{2+}$ ions, free $F^-$ ions and non bridging oxygens. The concentration of such bonding defects as mentioned above depends upon the concentration of $WO_3$.

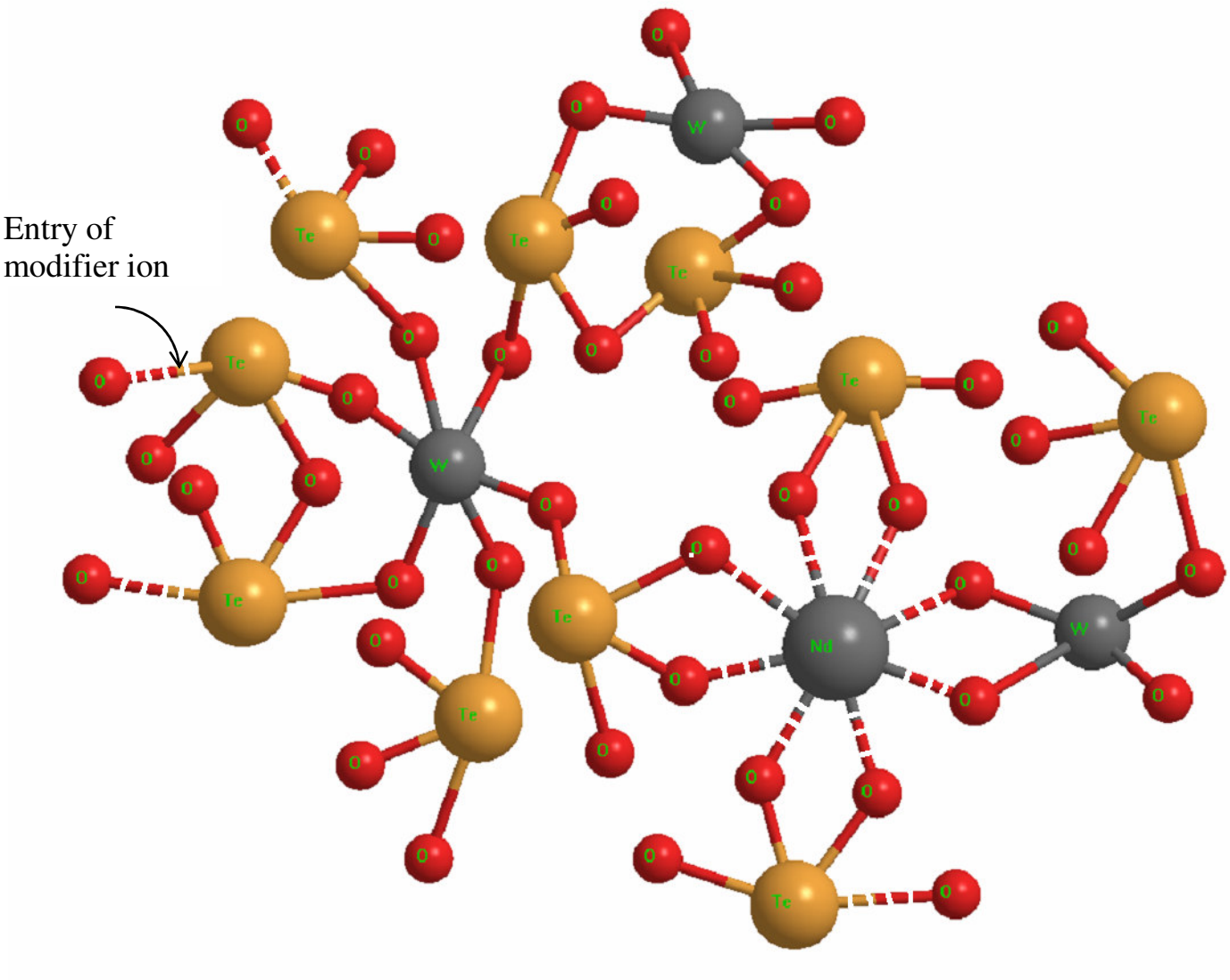


**Fig. 5.9** An illustration of $Nd^{3+}$ ion embedded in $TeO_2$ glass network with tungsten ions in tetrahedral and octahedral positions.

Thus, the variation in the concentration of $WO_3$ causes substantial structural modifications at the lasing ion site in $ZnF_2$–$WO_3$–$TeO_2$ glass network. If we consider the varying concentrations of tungsten ions of different valence states to be incorporated between the long-chain molecules in the vicinity of rare earth ion in the Te–O–Te network, then the symmetry and/or covalency of the glass at the rare earth ions should be different for the glasses containing different concentrations of $WO_3$ in the glass network. Additionally, the variations in the concentration of different structural units of tellurite, tungstenate and linkages between them are also expected to modify the crystal field around lasing ions in the glass network.

The rare earth ions that occupy different coordination sites with non–centro symmetric potential contribute significantly to $\Omega_2$. Even with similar coordination, the differences in the distortion at these ion sites may lead to a distribution in the local crystal field. The variations in the sites with non–centro symmetric potential (that may arise due to the influences of the dielectric of media, the environment of the rare earth ion and nephelauxetic effect) lead to changes in $\Omega_2$ value. In fact, among the three J–O parameters, the parameter $\Omega_2$ is related to the covalency and structural changes in the vicinity of the rare earth ion (short–range effect) and $\Omega_4$ and $\Omega_6$ are related the long-range effects and are strongly influenced by the vibrational levels associated with the central rare earth ions bound to the ligand atoms. The

comparison of $\Omega_2$ parameter for the three rare earth doped glasses shows the lowest values for glasses mixed with 15 mol % of $WO_3$.

According to the Judd–Ofelt theory, the intensity parameters contain two terms: (i). crystal field parameter that determines the symmetry and distortion related to the structural change in the vicinity of $Ln^{3+}$ ions. In the present context, this may be understood as follows: the higher the concentration of the modifier ions ($W^{5+}$ ions), the larger is the average distance between Te–O–W, Te–O–Te chains causing the average Ln–O distance to increase. Such increase in the bond lengths produces weaker field around $Ln^{3+}$ ions leading to a decrease in the value of $\Omega_2$ with increase in the concentration of $WO_3$. (ii) The covalency between the $Ln^{3+}$ ion and the ligand oxygen ion also contribute to $\Omega_2$. For oxide glasses this is related to the radial overlapping integral of the wavefunctions between 4f and admixing levels, e.g. 5d, 5g and the energy denominator between these two energy terms. Thus decreasing value of $\Omega_2$ with increase in the concentration of $WO_3$ up to 15 mol% points out, that there is a gradual increase in the concentration of $W^{5+}$ ions that act as modifiers in all the three series of the glasses. The values of $\Omega_4$ and $\Omega_6$ are strongly influenced by the vibrational levels associated with the central rare earth ions bound to the ligand atoms. The bonding parameter $\delta$ evaluated from the absorption data showed a decreasing trend with increase in the concentration of $WO_3$ up to 15 mol%. This observation indicates a decreasing

covalent environment for $Ln^{3+}$ ions from glass $LnW_5$ to $LnW_{15}$ and slightly higher covalent environment in glass $LnW_{20}$ with respect to that in $LnW_{15}$.

In the absorption spectra of $Nd^{3+}$ doped samples, the transition $^4I_{9/2} \rightarrow {}^4G_{5/2}$ is found to be more intense than any other state. This is evidently because of better validity of the selection rules, $\Delta J < 2$, $\Delta L < 2$ and $\Delta S = 0$, for this transition. In addition, the higher values of $\|U^{\lambda}\|^2$ are also considered as an important factor for the hyper sensitive nature of this level [129]. The positions of $^4I_{9/2} \rightarrow {}^4G_{5/2,}\ {}^4G_{7/2}$ transition of $Nd^{3+}$ are spectrally shifted towards slightly longer wavelength with the increase of $WO_3$ content. This observation indicates the dwindling of covalency of the chemical bond between the $Nd^{3+}$ and the ligand atoms [129]. This is also in accordance with the trend in $\Omega_2$. We have also observed the effective bandwidth of these transitions to be the highest for the glasses mixed with 15 mol% of $WO_3$. This observation points out that the distribution in the crystal fields due to differences in the site symmetries of $Nd^{3+}$ is narrower for the $NdW_{15}$ glass compared to the other three glasses in this series [130]. From the energy range of the transition $^4I_{9/2} \rightarrow {}^2P_{1/2}$ (23,200–23,400 $cm^{-1}$) observed, the effective coordination of this ion may be assumed between 8 and 9 in the studied glass network [18]. The eight coordination with $C_2$ symmetry may visualized by four pairs of oxide ions coming from four tetrahedral constituted by $TeO_4$ and $WO_4$ units as illustrated in Fig. 5.9.

The optical transitions $^6H_{5/2} \rightarrow {}^6F_{9/2}$, $^6F_{7/2}$ of $Sm^{3+}$ occurring in the absorption spectra in the near infrared region are hypersensitive. In the emission spectra of $Sm^{3+}$ ion, the transition $^4G_{5/2} \rightarrow {}^6H_{9/2}$ is also identified as hypersensitive. The closer observation of these spectra further indicates that $^6H_{5/2} \rightarrow {}^6F_{7/2}$ transition is a three fold triplet. Due to certain self adjustment of $Sm^{3+}$ environment in the glass network, there may be a degeneracy of $^6H_{5/2}$ ground state in the crystal field [131]; such degeneracy leads to the observed splitting of this transition. The luminescence spectra of $Sm^{3+}$ are similar to those reported for a number of other glass systems [131–133]. The high intensity of the luminescence bands of $Sm^{3+}$ ion in $SmW_{15}$ glass indicates the quenching of luminescence in this glass is low. The high luminescence output obtained for this glass also indicates that there is a less cross relaxation i.e., the transfer of energy from the excited state of Sm-ion by electric multipole interaction (more precisely dipole-dipole or dipole-quadrapole interactions) to neighboring Sm–ion lying in the ground state is low for this particular glass when compared with other glasses of this system. In the emission spectra, the transition $^4G_{5/2} \rightarrow {}^6H_{7/2}$ with $\Delta J = \pm 1$ is a magnetic dipole (MD) allowed where as the transition $^4G_{5/2} \rightarrow {}^6H_{9/2}$ is purely electric dipole one. The intensity ratio of electric dipole to magnetic dipole transitions is a measure of the asymmetry of the local environment of $Sm^{3+}$ ions. The greater the intensity ratio of the electric dipole transition to the magnetic dipole transition ($I_{4G5/2 \rightarrow 6H9/2}/I_{4G5/2 \rightarrow}$

$_{6H7/2}$) the more is the asymmetry of $Sm^{3+}$ in the network [21]. In the present work, this ratio is evidently more for the glass $SmW_{15}$ indicating the highest local disorder for the $Sm^{3+}$ ion in the network of this glass.

The absorption and emission spectra of $Eu^{3+}$ show special characteristics not exhibited by the other rare earth ions. The relative emission intensities of transitions occurring in the low energy region to those in the high energy region are quite sensitive to the host matrix. Hypersensitive transitions invariably appear, as intense emission bands in the low energy region and are influenced by micro-symmetry under-covalency of the rare earth ions. Further, the transition $^5D_0 \rightarrow {}^7F_0$ in the emission spectra is typical for coordination of the $Eu^{3+}$ ion. This transition observed at about 17, 200 $cm^{-1}$ for the studied glasses suggests 8-9 coordination for $Eu^{3+}$ ion in the glass network [134]. This transition is purely electric dipole in nature and can therefore be expected to give reliable values for the radiative parameters unlike other transitions which arise due to J mixing or pure magnetic dipole transitions. The transitions $^5D_0 \rightarrow {}^7F_2$ and $^5D_0 \rightarrow {}^7F_1$ occur in the red (R) and orange (O) regions, respectively and intensities of these transitions depend on the Judd-Ofelt parameters $\Omega_2$ and $\Omega_4$ or in other words the integrated emission intensity ratio of these two transitions (R/O ratio) is strongly influenced by site asymmetry (or structural changes in the vicinity of the $Eu^{3+}$ ion) and covalency of the bonds with the ligand anions [134, 135]. The values of this ratio shows a

decreasing trend ($EuW_5$ =5.32, $EuW_{10}$= 5.19, $EuW_{15}$= 4.92 and $EuW_{20}$ = 5.16) with the increase in the concentration of $WO_3$ up to 15 mol%, indicating decreasing covalent environment for $Eu^{3+}$ ions in this concentration range of $WO_3$.

The parameter $\beta_r$ (i.e., the branching ratio) of the luminescence transitions characterizes the lasing power of the potential laser transitions. The $\beta_r$ values obtained for various luminescent transitions for the three rare earth ions of the glasses mixed with 10 mol% of $WO_3$ are furnished in Tables 5.3 (a-c). It was well established that an emission level with $\beta_r$ value nearly equal to 50 % is a potential laser emission [136]. Among various transitions, the transitions $^4F_{3/2} \rightarrow {}^4I_{11/2}$, $^4G_{5/2} \rightarrow {}^6H_{7/2}$, $^5D_0 \rightarrow {}^7F_2$ respectively for $Nd^{3+}$, $Sm^{3+}$ and $Eu^{3+}$ doped glasses found to have the highest values of $\beta_r$ for all the three glasses; these transitions may therefore be considered as a possible laser transitions. Further, the comparison of $\beta_r$ values of these transitions for the glasses mixed with different concentrations of $WO_3$ shows the largest value for $LnW_{15}$ glasses indicating that these glasses exhibit better lasing action (Table 5.5).

The fluorescence decay curves of the emission lines corresponding to $^4F_{3/2}$ , $^4G_{5/2,}$ $^5D_0$ levels of $Nd^{3+}$, $Sm^{3+}$ and $Eu^{3+}$ ions respectively in $ZnF_2$-$TeO_2$ glasses mixed with different concentrations of $WO_3$ are recorded at room temperature and the log of intensity dependences with the decay time are

shown in Fig. 5.10; the variation indicates that the decay is single exponential. The fluorescence lifetime $\tau$, evaluated from these graphs is apparently shorter than calculated life times from the J–O theory (Table 5.5). Such difference may indicate on multi-phonon relaxations. The increasing trend of life time either calculated or measured for the glasses $LnW_5$ to $LnW_{15}$ suggests a decreasing trend of phonon loses or increasing presence of $W^{5+}$ ions that act as modifier in these glasses.

Normally, the non-radiative processes, the total radiative lifetime $\tau_m$ of particular level is defined as

$$\frac{1}{\tau_m} = A_{rad} + W_{mp} \tag{5.2}$$

where $A_{rad}$ is the radiative decay rate (in the absence of non-radiative losses) and $W_{mp}$ represents the multi-phonon decay rate of $Ln^{3+}$ ions given by

$$W_{mp}(T) = W_0 \left[ \frac{\exp(\hbar\omega / kT)}{\exp(\hbar\omega / kT) - 1} \right]^p \tag{5.3}$$

Where $W_0 = W_{mp}(T = 0\ K) = C \exp(-\alpha\Delta E)$.

$\Delta E$ is represents the gap between the levels of interest and p is the number of phonons given $\Delta E/\hbar\omega$.

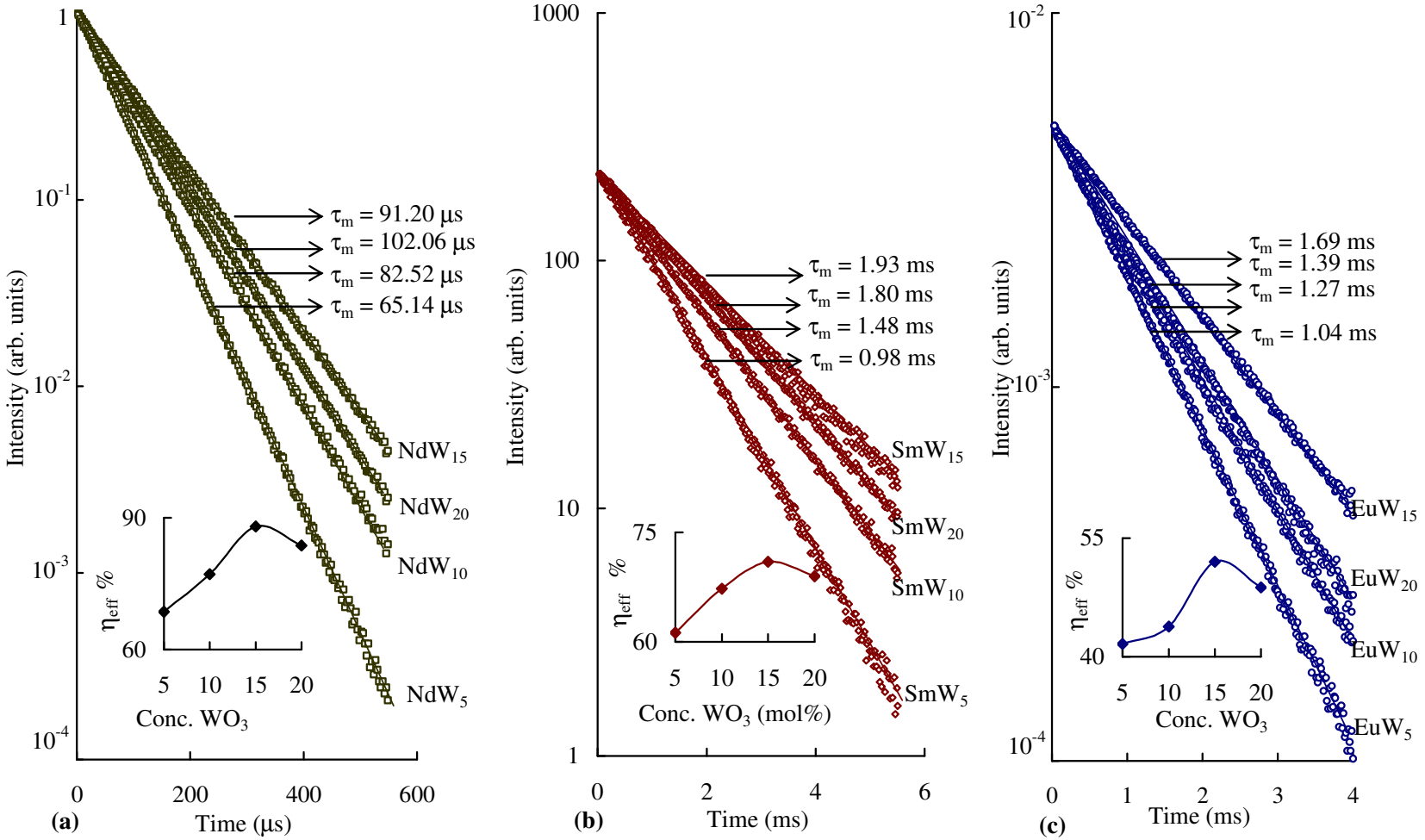


**Fig. 5.10** The variation of fluorescence intensity with the time of the emission lines of (a) $^4F_{3/2}$ ($Nd^{3+}$) , (b) $^4G_{5/2}$ ($Sm^{3+}$), (c) $^5D_0$ ($Eu^{3+}$) levels respectively in $ZnF_2$-$TeO_2$ glasses mixed with different concentrations of $WO_3$. Insets represent the variation of luminescence efficiency with the concentration of $WO_3$.

Additionally, some aggregations and interaction with the phonon subsystem may also be responsible for the observed variations in the radiative decay rate for these samples. Thus following the radiative life times, it is evident that there is a gradual decrease of interaction of $Ln^{3+}$ ions with the glass network in the glasses from $LnW_5$ to $LnW_{15}$ since $\tau_m$ is observed to increase with increase in the concentration of $WO_3$ up to 15 mol%.

The quantum yield ($\eta$) is defined as the radiative portion of the total relaxation rate of a given energy level [137]:

$$\eta = \frac{A_{rad}}{A_{rad} + W_{nr}} = \frac{\tau_{\exp}}{\tau_{rad}} \qquad (5.4)$$

where $A_{rad}$ is the total radiative relaxation rate, $W_{nr}$ is the rate of total non-radiative transition $\tau_{exp}$ –experimental lifetime, $\tau_{rad}$ –radiative lifetime. The value of $\eta$ for the three principal levels viz., $^4F_{3/2}$ , $^4G_{5/2,}$ $^5D_0$ of $Nd^{3+}$, $Sm^{3+}$ and $Eu^{3+}$ ions respectively are determined and presented in the Table 5.4. As the concentration of $WO_3$ is increased from 5 to 15 mol%, the value of $\eta$ is observed to increase considerably; such rise is connected not only with the rise of the radiative relaxation probability but also with a reduction of the non-radiative transition probability. This is possibly due to the decrease of the electron–phonon coupling of the $Ln^{3+}$ ion with the high-energy phonons and relative increase of this coupling with low-energy phonons in the $TeO_2$ glass network [138].

The radiative transition probabilities for all the three rare earth doped glasses mixed with 20 mol% of $WO_3$ show a deviation from those of the glasses $LnW_5$, $LnW_{10}$, $LnW_{15}$; such trend suggests that the reduction of tungsten ions to $W^{5+}$ state is considerably less in this glass. Major proportion exists in $W^{6+}$ states and participate in the glass network (this is also evidenced from IR, Raman and ESR spectral studies) causing to lower values of transition probabilities.

## 5.5 Conclusions

The optical absorption and photoluminescence spectra of $Nd^{3+}$, $Sm^{3+}$, $Eu^{3+}$ ions in $ZnF_2$–$TeO_2$ glasses mixed with different content of $WO_3$ have been reported. The Judd-Ofelt theory could successfully be applied to characterize the optical absorption spectra of these ions; out of the three J-O parameters ($\Omega_\lambda$), the value of $\Omega_2$, which is related to the structural changes in the vicinity of the $Ln^{3+}$ ion exhibited a gradual decrease with increase in the concentration of $WO_3$ up to 15 mol%. From this observation it is concluded that there is gradual increase in the degree of disorder or asymmetry in the glass network. The radiative transition probabilities and branching ratios evaluated for various luminescent transitions observed in the luminescence spectra, suggested the highest values for $^4F_{3/2}\rightarrow{}^4I_{11/2}$ ($Nd^{3+}$), $^4G_{5/2} \rightarrow {}^6H_{7/2}$ ($Sm^{3+}$) and $^5D_0\rightarrow{}^7F_2$ ($Eu^{3+}$). The comparison of $\beta_r$ values of these transitions showed the largest value for glass mixed with 15 mol% of $WO_3$. Finally, with the aid of the data on ESR, IR and

Raman spectral studies, it can be concluded that the glass containing around 15 mol% of $WO_3$ exhibits the highest luminescence efficiency for all the three rare earth ions.

## References


[1] I. Ardelean, S. Lupsor, D. Rusu, *Physica B* 405 (2010) 2259

[2] T. Hayakawa, M. Hayakawa, M. Nogami, P. Thomas, *Opt. Mater.* 32 (2010) 448

[3] D.K. Durga and N. Veeraiah, *J. Mater. Sci.* 36 (2001) 5625

[4] Y. Gandhi, N. Venkatramaiah, V. Ravikumar and N. Veeraiah, *Physica B* 404 (2009) 1450

[5] F. Chen, T. Xu, S. Dai, Q. Nie, X. Shen, J. Zhang, X. Wang, *Opt. Mater.* 32 (2010) 868

[6] J. Ozdanova, H. Ticha, L. Tichy, *Opt. Mater.*32 (2010) 950

[7] C. Laxmikanth, B.V. Raghavaiah, B. Appa Rao and N. Veeraiah, *J. Lumin.*109 (2004) 193

[8] I. Jlassi, H. Elhouichet, M. Ferid, R. Chtourou, M. Oueslati, *Opt. Mater.*32 (2010) 743

[9] G. Poirier, F. C. Cassanjes, Y. Messaddeq, S. J.L. Ribeiro, *J. Non-Cryst. Solids* 355 (2009) 441.

[10] C. Lasbrugnas, P. Thomas, O. Masson, J.C. Champarnaud-Mesjard, E. Fargin, V.Rodriguez, M. Lahaye, *Opt. Mater.* 31 (2009) 775.

[11] P. Subbalakshmi, N. Veeraiah, *J. Non-Cryst. Solids* 298 (2002) 89.

[12] Y. Gandhi, K.S.V. Sudhakar, M. Nagarjuna and N. Veeraiah, *J. Alloys Compd.* 485 (2009) 876

[13] Y.B. Saddeek, *Philos. Mag.* 89 (2009) 41.

[14] G. Liao, Q. Chen, J. Xing, H. Gebavi, D. Milanese, M. Fokine, M. Ferraris, *J. Non-Cryst. Solids* 355 (2009) 447.

[15] P. Chimalawong, J. Kaewkhao, C. Kedkaew, P. Limsuwan, *J. Phys. Chem. Solids* 71 (2010) 965

[16] J. Pisarska, W.A. Pisarski, W. Ryba-Romanowski, *Opt. Laser Tech.* 42 (2010) 805.

[17] K.B. Yatsimirskii, N.K. Davidenko, *Coord. Chem. Rev.* 27 (1979) 223

[18] L. Srinivasa Rao, M. Srinivasa Reddy, M.V. Ramana Reddy, N. Veeraiah, *Physica B* 403 (2008) 2542.

[19] R. Reisfeld, C.K. Jorgensen, *Lasers and Excited states of Rare Earths* (Springer- Verlag, New York, 1977).

[20] K. Hairao, S. Todoroki, D.H. Cho, N. Soga, *Opt. Lett*. 18 (1993) 1586.

[21] A. Kurita, T. Kushida, T. Izumitani, M. Matsukawa, *Opt. Lett.* 19 (1994) 314.

[22] K.K. Mahato, D.K. Rai, S.B. Rai, *Solid State Commun.* 108 (1998) 671.

[23] J. Zhang, D.L. Yang, E.Y.B. Pun, H. Gong, H. Lin, *J. Appl. Phys.* 107 (2010) 123111

[24] K.S.V. Sudhakar, M. Srinivasa Reddy, L. Srinivasa Rao and N. Veeraiah, *J. Lumin.* 128 (2008) 1791

[25] Z. Mazurak, S. Bodył, R. Lisiecki, J. Gabryś-Pisarska, M. Czaja, *Opt. Mater*. 32 (2010) 547

[26] G. Lakshminarayana, R.Yang, M.Mao, J. Qiu, I.V. Kityk, *J. Non-Cryst. Solids* 355 (2009) 2668.

[27] R. Reisfeld, *Structure and Bonding* 22 (Springer-Verlag, New York, 1975).

[28] D.E. Henrie, R.L. Fellows, G.R. Choppin, *Coord. Chem. Rev*. 18 (1976)199.

[29] W.D. Horrocks, Jr. and M. Albin, *Prog. Inorg. Chem.* 31 (An Interscience Publication, New York, 1984) 1.

[30] K. Hirao, S. Todoroki, N. Soga, *J. Non-Cryst. Solids* 175 (1994) 263.

[31] G. Boulon, M. Bouderbala, J. Seriot, *J. Less-common Metals*. 112 (1985) 41.

[32] M. Nogami, A. Ohno, H. You, *Phys. Rev. B* 68 (2003) 104204

[33] C. Shen, S. Baccaro, Z. Xing, Q. Yan, S. Wang, G. Chen, *Chem. Phys. Lett*. 492 (2010) 123

[34] V. Ravikumar, N. Veeraiah and B. Appa Rao, *J. Mater. Sci.* 33 (1998) 2659.

[35] J. Ozdanova, H.Ticha, L.Tichy, *J. Non-Cryst. Solids* 355 (2009) 2318.

[36] D. Munoz-Martín, M.A. Villegas, J. Gonzalo, J.M. Fernández-Navarro, *J. Euro. Ceram. Soc.* 29 (2009) 2903.

[37] S. Surendra Babu, R. Rajeswari, K. Jang, C. Eun Jin, K. Hyuk Jang, H. Jin Seo, C.K. Jayasankar, *J. Lumin.* 130 (2010) 1021.

[38] H. Cankaya, A. Sennaroglu, *Appl. Phys. B* 99 (2010) 121.

[39] S.A. Saleem, B.C. Jamalaiah, J.S. Kumar, A.M. Babu, L.R. Moorthy, M. Jayasimhadri, K. Jang, (...),J.H. Jeong, *Solid State Sci.* 11 (2009) 2093.

[40] H. Zhong, B. Chen, G. Ren, L. Cheng, L. Yao, J. Sun, *J. Appl. Phys.* 106 (2009) 083114

[41] R.K. Verma, K. Kumar, S.B. Rai, *Spectrochim. Acta - Part A* 74 (2009) 776.

[42] L.C. Courrol, L.R.P. Kassab, V.D.D. Cacho, S.H. Tatumi, N.U. Wetter, *J. Lumin*. 102 (2003) 101

[43] B. Wilhelm, V. Romano, H.P. Weber, *J. Non-Cryst. Solids* 328 (2003) 192.

[44] B. Karthikeyan, S. Mohan, *Physica B* 334 (2003) 298.

[45] K. Annapurna, R.N. Dwivedi, P. Kundu, S. Buddhudu, *Mater. Lett.* 57 (2003) 2095.

[46] M.B. Saisudha, J. Ramakrishna, *Opt. Mater.* 18 (2002) 403.

[47] S. Shen, A. Jha, E.Zhang, S.J. Wilson, *Comptes Rendus Chimie* 5 (2002) 921.

[48] G.A. Kumar, A. Martinez, E.De La Rosa, *J. Lumin.* 99 (2002) 141.

[49] Feng Chen, Xue-Lin Wang, Xi-Shan Li, Li-Li Hu, Qing-Ming Lu, Ke-Ming Wang, Bo Rong Shi, Ding-Yu Shen, *Appl. Surface Science* 193 (2002) 92.

[50] C.H. Kam, S. Buddhudu, *Opt. Lasers in Engg*.35 (2001) 11

[51] E. De la Rosa-Cruz, GH.A. Kumar, L.A. Diaz-Torres, A. Martinez, O. Barbosa Garcia, *Opt. Mater.* 18 (2001) 321.

[52] J. Fernandez, R. Balda, M. Sanz, L.M. Lacha, A. Oleagha, J.L. Adam, *J. Lumin*. 94 (2001) 325.

[53] R. Balda, L.M. Lacha, A. Mendioroz, M. Sanz, J. Fernandez, J.L. Adam, M.A. Arriandiaga, *J. Alloys Comp.* 323 (2001) 255.

[54] S.S.L. Surana,Y.K. Sharma, S.P. Tandon, *Mater. Sci. Engg. B* 83 (2001) 204.

[55] G. V. Prakash, *Mater. Lett.* 46 (2000) 15.

[56] T.V.R. Rao, R.R. Reddy, Y. Nazeer Ahammed, M. Parandamaiah, N. Sooraj Hussain, S. Buddhudu, K. Purandar, *Infrared Phys. & Tech.* 41 (2000) 247.

[57] Q. Xiang, Y. Zhou, Y.L. Lam, Y.C. Chan, C.H. Kam, B.S. Ooi, H.X. Zhang, S. Buddhudu, *Mater. Res. Bull.* 35 (2000) 571.

[58] M. Bouderbala, H. Mohmoh, A. Bahtat, M. Bahtat, M. Ouchetto, M. Druetta, B. Eloudai, *J. Non-Cryst. Solids* 259 (1999) 23.

[59] Fabia C. Cassanjes, Younes Messaddeq, Luiz F.C. de Oliveria, Lilia C. Courrol, Laercio Gomes, Sidney J.L. Ribeiro, *J. Non-Cryst. Solids* 247 (1999) 58.

[60] V. Mehta, G. Aka, A.L. Dawar, A. Mansingh, *Opt. Mater.* 12 (1999) 53.

[61] V. Mehta, D. Gourier, A.L. Dawar, A. Mansingh, *Solid State Commun.* 109 (1999) 513.

[62] V.V. Ravi Kanth Kumar, Anil K. Bhatnagar, *Opt. Mater.* 11 (1998) 41.

[63] A. Srinivasa Rao, J. Lakshmana Rao, Y. Nazeer Ahammed, R. Ramakrishna Reddy, T.V. Ramakrishna Rao, *Opt. Mater.* 10 (1998) 129.

[64] G. Ajit Kumar, P.R. Biju, C. Venugopal, N.V. Unnikrishnan, *J. Non-Cryst. Solids* 221 (1997) 47.

[65] B.C. Joshi, R. Lohani, *J. Non-Cryst. Solids* 215 (1997) 103.

[66] A.L. Dawar, V. Mehta, Abhai Mansingh, Raj Rup, *Opt. Mater.* 7 (1997) 33.

[67] Ning Lei, Bing Xu, Zhonghong Jiang, *Opt. Commun.* 127 (1996) 263.

[68] Giorgio Pozza, David Ajo, Marco Bettinelli, Adolfo Speghini, Maurizio Casarin, *Solid State Commun.* 97 (1996) 521.

[69] Y.C. Ratnakaram, S. Buddudu, *Solid State Commun.* 97 (1996) 651.

[70] S. Sen, J.F. Stebbins, *J. Non-Cryst. Solids* 188 (1995) 54.

[71] H. Ebendorff-Heidepriem, W. Seeber, D. Ehrt, *J. Non-Cryst. Solids* 183 (1995) 191.

[72] S. Shanmuga Sundari, K. Marimuthu, M. Sivraman, S.S. Babu, *J. Lumin.* 130 (2010) 1313

[73] A. Agarwal, I. Pal, S. Sanghi, M.P. Aggarwal, *Opt. Mater.* 32 (2009) 339.

[74] N. Sooraj Hussain, G. Hungerford, R. El-Mallawany, M.J.M. Gomes, M.A. Lopes, N. Ali, J.D. Santos, S. Buddhudu, *J. Nanosci. Nanotech.* 9 (2009) 3672.

[75] D. Udaya Bhaskar, S. Buddhudu, *Ferroelect. Lett*.33 (2006) 57.

[76] P.R. Biju, G. Jose, P.V. Jyothy, *J. Mod. Opt.* 52 (2005) 2687.

[77] C.K. Jayasankar, E. Rukmini, *Opt. Mater.* 8 (1997) 193.

[78] C.K. Jayasankar, V. Venkatramu, P. Babu, Th. Troster, W. Sievers, G. Wortmann, W. B. Holzpfel, *J. Appl. Phys*. 97 (2005) 093523.

[79] A Kumar, D.K. Rai, S.B. Rai, *Spectrochim. Acta A* 59 (2003) 917.

[80] K. Kojima, A. Kubo, M. Yamashita, N. Wada, T. Tsuneoka, Y. Komatsubara, *J. Lumin*. 87 (2000) 697.

[81] A.G. Souza Filho, P.T.C .Freire, I.Guedes, F.E.A. Melo, J.J.Mendes Filho, M.C.C.Custodio, R.Lebullenger, A.C. Hernandes, *J. Mater. Sci. Lett.* 19 (2000) 135.

[82] K. Annapurna, R.N. Dwivedi, A. Kumar, A.K. Chauduri, S. Buddhudu, *Spectrochim. Acta,* 56 (2000) 103.

[83] G.K.D. Mahapatra, *Phys. Chem. Glasses* 40 (1999) 57.

[84] Y. Shimizugava, N. Umesaki, K. Hanada, I. Sakai, J. Qiu, *J. Synchrotron Rad.* 8 (2001) 797.

[85] Y. Shimizugava, N. Sawaguchi, *J. Appl. Phys.* 81 (1997) 6657.

[86] M.C. Farries, P.R. Morkel, J.E. Townsend, *Elect. Lett*. 24 (1988) 709.

[87] L.R.P. Kassab, D.S. Da Silva, C.B. De Araújo, *J. Appl. Phys.* 107 (2010) 113506

[88] C. Zhu, A. Monteil, M. Ei-Jouad, N. Gaumer, S. Chaussedent*, J. Am. Ceram. Soc.* 93 (2010) 1039

[89] H.Q. Liu, *J. Hunan Univ. Nat. Sci.* 37 (2010) 66.

[90] W. Xu, C.R. Li, B.J. Chen, Z.Q. Feng, *Acta Phys. Sinica* 59 (2010) 1328

[91] A.P. Carmo, M.J.V. Bell, V. Anjos, R. De Almeida, D.M. Da Silva, L.R.P. Kassab, *J. Phys. D* 42 (2009) 155404

[92] C. H. Kam, S. Buddhudu, *Physica B* 344 (2004) 182.

[93] J. Wasylak, K. Ozga, I.V. Kityk, J. Kucharski, *Infrared Physics & Tech.* 45 (2004) 253.

[94] P. R. Biju, G. Jose, V. Thomas, V. P. N. Nampoori, N. V. Unnikrishnan, *Opt. Mater*. 24 (2004) 671.

[95] W.D. Fragosoa, Celso Mello Doneg, R. L. Longo, *J. Lumin.* 105 (2003) 97.

[96] S. Awomir, M. Kaczmareka, T. Tsuboi, G. Boulonc, *Opt. Mater.* 22 (2003) 303.

[97] V. Lavin, U. R. Rodriguez-Mendoza, I. R. Martin, V. D. Rodriguez, *J. Non-Cryst. Solids* 319 (2003) 200.

[98] T. Kushida, A. Kurita, M. Tanaka, *J. Lumin.* 102 (2003) 301.

[99] R. R. Reddy, Y. Nazeer Ahammed, K. Rama Gopal, T. V. R. Rao, P. Abdul Azeem, S. Buddhudu, N. Sooraj Hussain, *J. Quant. Spectr. Rad. Tran.* 75 (2002) 507.

[100] Akshaya Kumar, S. B. Rai, *Spectrochim. Acta Part A* 58 (2002) 2115.

[101] H. Xia, J. Wang, Q. Nie, H. Song, *Mater. Lett.* 53 (2002) 277.

[102] K. Annapurna, S. Buddhudu, *Mater. Lett*. 53 (2002) 359.

[103] A. J. Silversmith, D. M. Boyeb, R. E. Andermana, K. S. Brewera, *J. Lumin.* 94 (2001) 275.

[104] N. Sooraj Hussain, Y. Prabhakara Reddy, S. Buddhudu, *Mater. Res. Bull.* 36 (2001) 1813.

[105] I.V. Kityk, J. Wasylak, D. Dorosz, J. Kucharski, *Opt. Laser Techn.* 33 (2001) 157.

[106] P. Babu, C. K. Jayasankar, *Physica B* 279 (2000) 262.

[107] E. Culea, T. Ristoiu, I. Bratu, *Mat. Sci. Engg. B* 75 (2000) 82.

[108] M. Bettinelli, A. Speghini, M. Ferrari, M. Montagna, *J. Non-Cryst. Solids* 201(1996) 211.

[109] V. Aruna, N. Sooraj Hussain, K. Rajamohan Reddy, K. Annapurna, S. Buddhudu, Mater. Lett., 33 (1997) 201.

[110] A. C. Vaz, de Arafijo, I. T. Weber, B. S. Santos, B. J. P. da Silva, R. P. de Mello Jr., S. Alves Jr., G. F. de Sit, C. de Mello Donegfi, *J. Non-Cryst. Solids* 219 (1997) 160.

[111] R. Jagannathan, K. Athinarayanasamy, A. Mani, C. K. Jayasankar, *Opt. Mater.* 5 (1996) 574.

[112] I. Morozova, A. Yakind, *Fis. Khim. Stekla* 3 (1977) 197.

[113] K.J. Rao, *Structural Chemistry of Glasses*, Elsevier, Amsterdam, 2002.

[114] G. Upender, C.P. Vardhani, S. Suresh, A.M. Awasthi, V. Chandra Mouli, *Mater. Chem. Phys.* 121 (2010) 335

[115] Z. Pan, D.O. Henderson, S.H. Morgan, *J. Non-Cryst. Solids* 171 (1994) 134.

[116] T. Sekiya, N. Mochida, A. Ohtsuka, T. Tonokawa, *J. Non-Cryst. Solids* 144 (1992) 128.

[117]H. Burger, K. Kneipp, H. Hobert*, J. Non-Cryst. Solids* 151 (1992) 134.

[118]B.V.R. Chowdari, P. Pramoda Kumari, *Solid State Ionics* 113 (1998) 665.

[119]A. Goldstein, V. Chiriac, D. Becherescu, *J. Non-Cryst. Solids* 92 (1987) 271.

[120]P. Subbalakshmi, B.V. Raghavaiah, R. Balaji Rao and N. Veeraiah, EPJ *Appl. Phys.* 26 (2004) 169

[121]B.M. Walsh, "*Judd-Ofelt Theory: Principles and Practices*" in Advances in Spectroscopy for Lasers and Sensing, ed. B. Di Bartolo and O. Forte (Springer, Netherlands, 2006) 403-433.

[122]C.K. Jorgenson, in: *Orbitals Atoms and Molecules*, Academic Press, London, 1962.

[123]S.P. Sinha, in: *Complexes of the Rare Earths*, Pergamon, Oxford, 1966.

[124]V. Dimitrov, M. Arnaudov, Y. Dimitriev, *Monatsh. Chem., Chem. Mon*. 115 (1984) 987.

[125]K. Sambasiva Rao, M. Srinivasa Reddy, V. Ravi Kumar, N. Veeraiah, *Mater. Chem. Phys.* 111 (2008) 283.

[126]S. Muthupari, S. Prabakar, K.J. Rao, *J. Phys. Chem. Solids* 57 (1996) 553.

[127]A. Brenier, I.V. Kityk*, J. Appl. Phys.* 90 (2001) 232.

[128]S.M.D. Nery, W.M. Pontuschka, S. Isotani, C.G. Rouse, *Phys. Rev. B* 49 (1994) 3760.

[129]J. Lucas, *J. Less Comm. Metals.* 112 (1985) 27.

[130]K.B. Yatsimirskii, N.K. Davidenko, *Coord. Chem. Rev*. 27 (1979) 223

[131]H. Ahrens, M. Wollenhaupt, P. Frobel, J. Lin, K. Barner, G.S. Sun, R. Braunstein, *J. Lumin.* 82 (1999) 177.

[132]A.G.S. Filho, J.M. Filho, F.E.A. Melo, M.C.C. Custodio, R. Lebullenger, A.C. Hernandes*, J. Phys. Chem. Solids.* 61 (2000) 1535.

[133] K. Devlin, B. O' Kelly, Z.R. Tang, C. Mc. Donagh, J.F. Mc. Glip, *J. Non-Cryst. Solids* 135 (1991) 8.

[134]Q. Su, Z. Pei, L. Chi, H. Zhang, Z. Zhang, F. Zou, *J. Alloys Compds.* 192 (1993) 25.

[135]E.W.J.L. Oomen, A.M.A. va Dongen, *J. Non-Cryst. Solids* 111 (1989) 205.

[136]C. Hirayama, F.E. Camp, N.T. Melamid, K.B. Steinbruegge, *J. Non-Cryst. Solids* 6 (1971) 342.

[137]M. Rozanski, K. Wisniewski, J. Szatkowski, Cz. Koepke, M. Sroda, *Opt. Mater.* 31 (2009) 548.

[138]R. Lam, T. Langet, J.E. Greedan, *J. Solid State Chem.* 171 (2003) 317.